学位論文

Regulatory mechanism for the motility in hamster spermatozoa
（ハムスター精子鞭毛の運動性調節機構の解析）

東京大学大学院 新領域創成科学研究科
先端生命科学専攻 資源生物制御学分野

絹川 将史

Table of Contents

Abstract

In the present study, I investigated the mechanisms by which microtubule sliding is converted into flagellar bending and then flagellar bending generates the motility of spermatozoa. Hyperactivation is a good model for investigation of the mechanism by which flagellar bending generates the motility of spermatozoa, since the propulsive force for the movement is enhanced. To investigate this mechanism, I quantitatively analyzed the motility and flagellar bending in hyperactivated hamster spermatozoa. I also used the demembranated spermatozoa model to investigate the mechanism by which microtubule sliding is converted into flagellar bending.

In chapter 1, I quantitatively analyzed the changes in the motility pattern of hamster spermatozoa during the course of hyperactivation. In the culture system used in this study, hyperactivation spontaneously occurred 4 h after incubation *in vitro*. Several parameters were examined in the analysis of the movement pattern. Curvilinear velocity, average path velocity, and straightness abruptly changed between 2 and 4 h of incubation. However, linearity, amplitude of lateral head displacement, beat frequency, and average wavelength gradually changed with time. These results indicate that complex physiological changes occur before hyperactivation. The phosphorylation levels of some proteins were changed gradually or abruptly during the incubation up to 4 h, which corresponded to the gradual or abrupt changes in the motility pattern, respectively. These results suggest that protein phosphorylation is involved in the regulation of motility in spermatozoa. In addition, the ability of spermatozoa to swim in a viscoelastic medium increased between 2 and 4 h, suggesting that the propulsive force in swimming was enhanced upon the occurrence of hyperactivation.

In chapter 2, to clarify the mechanism by which flagellar bending efficiently generates the propulsive force, I examined the flagellar bending in hyperactivated and non-hyperactivated spermatozoa and compared them. In the analysis for flagellar bending, the bend angles were measured after dividing the images of the flagellum into

short lengths. Flagellar bending changed in different manners in each region during incubation. The asymmetry to the direction of the curve of the head gradually increased with time in the first half of the flagellum. The flexibility abruptly decreased between 10 min and 1 h, and then increased between 2 and 4 h in the first half of flagellum. In the analysis for the propagation of wave, I found that additional small waves occurred in the mid region and were propagated to the distal region in the spermatozoa incubated for 10 min but not for 4 h. The additional wave seems to interfere in the formation of complete cycle of the large waves to reduce the propulsive force. Finally, in the analysis for the bending rate, I identified the effective and ineffective stroke for the progressive movement by the calculation of the propulsive force on each position along with whole flagellum. When the effective stroke generates the propulsive force, the high amplitude would be an important determinant for generating the large propulsive force.

In chapter 3, to clarify the mechanism by which microtubule sliding is converted into flagellar bending, I examined microtubule sliding and flagellar bending separately by using the demembranated spermatozoa model. To examine the microtubule sliding, I developed a novel method using a high concentration of reducing agent by which microtubules were efficiently extruded. Using these methods, I examined the roles of cAMP, Ca^{2+}, and their target kinases in the regulation of flagellar bending and microtubule sliding. The microtubule extrusion but not flagellar bending occurred without cAMP in the reactivation medium, suggesting that cAMP regulates the conversion of microtubule sliding into flagellar bending but not microtubule sliding itself. The target of cAMP was not cAMP dependent protein kinase (PKA), because H89, a potent inhibitor of PKA, did not inhibit flagellar bending. Alternatively, Epac2/Rap2 pathway would mediate the signal of cAMP to regulate flagellar bending. Immunoblotting analysis demonstrated that Epac2 and Rap2 are present in the hamster spermatozoa. Since the microtubule extrusion but not flagellar bending occurred at 10^{-4}-10^{-3} M of Ca^{2+}, Ca^{2+} seems to down-regulate the conversion of microtubule sliding into flagellar bending. The target of Ca^{2+} was neither Ca^{2+} dependent protein kinase

(PKC) nor calmodulin, because neither of their inhibitors attenuated the inhibition of flagellar bending by Ca^{2+}. Finally, an inhibitor of PKC completely inhibited the microtubule extrusion in a Ca^{2+}-free condition, suggesting that PKC is involved in the regulation of microtubule sliding independently of Ca^{2+}.

In this thesis, I investigated the mechanisms regulating two processes in which the motility is generated in hamster spermatozoa. First, I investigated the process in which flagllar bending generates the motility in spermatozoa. In the analysis of this process, I characterized the patterns of movement and flagellar bending in hyperactivated spermatozoa and elucidated how they produce the large propulsive force. Second, I investigated the process in which microtubule sliding is converted into flagellar bending. In the analysis of this process, I found that cAMP, Ca^{2+}, and their target proteins distinctly regulate the microtubule sliding and the conversion of microtubule sliding into flagellar bending. It is thus important in elucidating the molecular mechanisms regulating the motility of spermatozoa to separately analyze the microtubule sliding and flagellar bending.

General Introduction

Fertilization is one of the attractive phenomena which have been studied by many researchers. Spermatozoa are the one of two principal parts in fertilization and their role is to bring a haploid genome into the egg. For this purpose spermatozoa are necessary to swim actively to reach an oocyte. Therefore, it is important in understanding the whole processes of fertilization to elucidate the mechanism regulating spermatozoa motility.

The motility of spermatozoa for progressive swimming is generated by flagellar bending, which is regulated *via* the activation of the flagellar axoneme. The typical structure of the flagellar axoneme in most eukaryotic flagella is that of a central pair of singlet microtubule, which is surrounded by nine doublet microtubules (9+2 arrangement). Flagellar bending is generated by the sliding of adjacent doublet microtubules *via* the activity of dynein arm ATPase, using Mg^{2+}-ATP as the substrate (Lindemann and Gibbons, 1975; Shingyoji *et al*, 1977). Although the mechanism regulating microtubule sliding has been well studied (see review: Woolley, 2000; Inaba, 2003), little is known about the mechanisms by which microtubule sliding is converted into flagellar bending and then flagellar bending generate spermatozoa motility. It is important in understanding the whole regulations of spermatozoa motility to elucidate these mechanisms.

Hyperactivated spermatozoa is a good model for the investigation of the mechanism by which flagellar bending generate spermatozoa motility. Hyperactivation, which was termed by Yanagimachi (1981), is a phenomenon that spermatozoa dramatically change their motility pattern around the time of capacitation *in vivo* (Katz and Yanagimachi, 1980; Suarez and Osman, 1987) and *in vitro* (Yanagimachi, 1970; Fraser, 1977; Katz *et al*., 1978; Katz and Yanagimachi, 1980; Suarez *et al*., 1983; Suarez and Osman, 1987; Morales *et al*., 1988; Shivaji *et al*., 1995; Ishijima *et al*., 2002). The motility pattern of mammalian spermatozoa converts into vigorous and not straight

swimming pattern upon the occurrence of hyperactivation. Although the changes in hyperactivated spermatozoa motility are closely examined in many species, the changes in flagellar bending has not been well examined. In hyperactivated spermatozoa, amplitude and asymmetry increase in flagellum (Ishijima and Mohri, 1985; Katz *et al*., 1986; Suarez, 1988; Suarez *et al*., 1991; Aoki *et al*., 1994). However the relationship between flagellar bending and progressive motility in spermatozoa remains unclear. There are many reports in which simulation models of spermatozoa movement were created to explain the mechanism by which flagellar bending generate the progressive motility (Gray, 1955; Gray 1958; Brokaw, 2002). In these models, however, bending pattern of flagellum was approximated by sine curve. These simulations can not be applied in hyperactivated rodent spermatozoa, since the waveform of flagellar bending is asymmetrical (Aoki *et al*., 1994). Therefore, the detailed analysis for the flagellar bending is important in elucidating the regulation of spermatozoa motility in hyperactivated spermatozoa.

There are many reports suggesting that various factors are involved in the regulation of spermatozoa motility. Especially, protein phosphorylation could be an important post-translational event regulating spermatozoa motility *via* Ca^{2+} and cAMP as second messengers. The role of Ca^{2+} on the regulation of flagellar movement has been investigated by many researchers (Brokaw *et al*, 1974; Bessen *et al*., 1980; Gibbons and Gibbons, 1980; Gibbons, 1982; Kamiya and Witman, 1984; Bannai *et al*., 2000). Ca^{2+} induced asymmetrical bending waves in demembranated sea urchin spermatozoa (Brokaw, 1979). Calmodulin and calmodulin-dependent protein kinase II, which is a target of Ca^{2+}, induce the motility in *Chlamydomonas* flagellum (Smith, 2002) and *ascidian* spermatozoa (Nomura *et al*., 2004). Cyclic AMP plays important roles in the initiation of spermatozoa swimming. The concentration of cAMP abruptly increased in mammalian and starfish spermatozoa when they were released into the physiological medium (Ishida *et al*., 1987; Niitus-Hosoya *et al*., 1987; White and Aithen, 1989). When rainbow trout spermatozoa initiate swimming, a 15 kDa protein is

phosphorylated on tyrosine residue and this phosphorylation is dependent on cAMP (Morisawa and Hayashi, 1986; Hayashi *et al*., 1987) which regulate the spermatozoa motility *via* the activation of cAMP dependent protein kinase and the stimulation of protein phosphorylation (Brandt and Hoskins, 1980; Noland *et al*., 1987; Bookbinder *et al*., 1991).

Microtubule extrusion in the demembranated spermatozoa is a good model system for the investigation of the mechanism by which microtubule sliding is converted into flagellar bending. In the previous study, microtubule extrusion was examined by the treatment with protease such as trypsin (Summers and Gibbons, 1973; Brokaw and Simonick, 1977; Olson and Linck, 1977; Si and Okuno, 1993; Si and Okuno, 1995) and elastase (Brokaw, 1980; Ishijima *et al*., 2002). Using this method, Ca^{2+} is suggested to play an important role in the regulation of microtubule sliding (Wargo and Smith, 2003; Nakano *et al*., 2003). Cyclic AMP may also be essential for microtubule sliding. Cyclic AMP is required for the reactivation of the demebranated spermatozoa motility in boar (Lindemann, 1978; Ishida *et al*., 1987), dog (Tash *et al*., 1984; Tash *et al*., 1986), and hamster (Ishida *et al*., 1987). However, since it seems likely that proteases degrade important regulatory components involved in flagellar bending as well as the proteins connecting microtubules, it is not adequate to use the enzymes for the investigation of microtubule sliding. Due to the absence of useful method for analyzing microtubule sliding, the mechanism by which microtubule sliding is converted into flagellar bending could not have been well studied.

The purpose of this study is to elucidate the whole regulatory mechanism for spermatozoa motility. To this end, I analyzed the flagellar bending in hyperactivated hamster spermatozoa to elucidate the mechanism by which flagellar bending generates spermatozoa motility. In addition, I developed a novel method for microtubule extrusion with minimal digestion of proteins. Using this method, I investigated the effect of Ca^{2+} and cAMP on microtubule extrusion to investigate the mechanism by which microtubule sliding is convert into flagellar bending. In Chapter 1, the precise characteristics of

hyperactivated motility were examined and the physiolosical significance of hyperactivation was clarified. In Chapter 2, the flagllar bending was analyzed in hyperactivated spermatozoa. Finally in Chapter 3, the effect of PKC or PKA for spermatozoa motility and microtubule extrusion was examined. I used hamsters as an experimental animal by the following reasons. Firstly the shape of the heads in rodent spermatozoa is like a hook and useful to determine the direction of flagellar bending. Secondly the waveform is two dimensional, which make it easy to analyze the flagellar bending under a phase-contrast microscope.

Chapter 1

Analysis of the motility during the course of hyperactivation in hamster spermatozoa

Abstract

The motility pattern of mammalian spermatozoa changes during migration in the female genital tract and during incubation *in vitro*. This change in motility is termed hyperactivation. Hyperactivated spermatozoa swim vigorously in 'whiplash', 'figure-8', or 'small circle' trajectories. In this study, a quantitative analysis was carried out of the changes in the motility pattern of hamster spermatozoa during incubation to investigate the mechanism regulation hyperactivation. In the culture system used in this study, hyperactivation occurred 4 h after incubation. Several parameters in the analysis of spermatozoa movement pattern were examined. Curvilinear velocity, average path velocity, and straightness abruptly changed between 2 and 4 h. However, linearity, amplitude of lateral head displacement, beat frequency, and average wavelength gradually changed with time. These results indicate that complex physiological changes occur before hyperactivaion. The ability of spermatozoa to swim in a viscoelastic medium increased between 2 and 4 h, suggesting that the power of movement was enhanced during this period. This result suggested that hyperactivation was the physiologically significant event, since spermatozoa need to swim in a viscoelastic environment in the oviduct and around eggs before fertilization. Spermatozoa proteins with molecular masses of 86 and 75 kDa were phosphorylated at tyrosine residues and the phosphorylation level increased with time. These proteins may be involved in the gradual changes in the motility pattern. A 41-kDa protein was phosphorylated at serine/threonine residues and the phosphorylation level increased between 10 min and 1 h and then decreased between 2 and 4 h. This protein may be involved in the abrupt changes in motility pattern.

Introduction

The motility pattern of mammalian spermatozoa changes before fertilization. Freshly ejaculated mammalian spermatozoa are actively motile, but are unable to fertilize an oocyte. Spermatozoa need to spend a period of time in either the female reproductive tract or an appropriate *in vitro* environment to become competent for fertilization. During this period, spermatozoa undergo a physiological change termed capacitation. This is a prerequisite for the acrosome reaction (Yanagimachi, 1994). At the same time as spermatozoa undergo capacitation *in vitro*, their swimming pattern changes. They swim more vigorously than before, in 'whiplash', 'figure-8' or 'small circle' trajectories. This change in sperm motility around the time of capacitation seems to be common in mammalian species, and has been termed hyperactivation (Yanagimachi, 1981). A common feature of hyperactivated spermatozoa motility in all species examined is that the spermatozoa do not swim in a straight line: in some species they swim in a zig-zag trajectory and in others they swim in small circles. In microscopic observations, the change to the hyperactivated motility pattern seems to occur abruptly (Yanagimachi, 1970), although in hamster spermatozoa the ratio for several motility patterns of planar, circular, helical and hatchet changed over time (Shivaji *et al*., 1995). The motility of hyperactivated spermatozoa has been analyzed using computer assisted spermatozoa analysis (CASA) in various species, for example mice (Neill and Olds-Clarke, 1987), humans (Mortimer and Swan, 1995), sheep (Mortimer and Maxwell, 1999) and rats (Cancel *et al*., 2000). In CASA analysis, these patterns have been compared in freshly collected and hyperactivated spermatozoa, but have not been examined over time, as hyperactivation appears to occur abruptly. However, in elucidating the mechanism of hyperactivation, it is important to examine the time-dependent changes in these parameters.

Hyperactivation is a necessary event for spermatozoa to achieve successful fertilization. Using various methods that prevented hyperactivation but did not inhibit

the acrosome reaction, it was shown that hyperactivated hamster spermatozoa were more successful in fertilization *in vitro* than those that were not hyperactivated (Stauss *et al*., 1995). However, it is not clear how hyperactivated motility is necessary for fertilization. After ejaculation into the genital tract, spermatozoa pass through the isthmus of oviducts and reach the ampulla of uterine tube where they fertilize eggs. The pathway is a highly viscoelastic environment derived from the oviductal mucus and cumulus matrix (Drobnis *et al*., 1988; Yudin *et al*., 1988). However, in almost all previous studies, the motility of spermatozoa was examined in the medium with low viscosity, which would not reflect the physiological condition.

The mechanism that brings about hyperactivation remains to be established. Extracellular Ca^{2+} is required to maintain hyperactivated motility pattern in hamster spermatozoa *in vitro* (Yanagimachi, 1994). Increased intracellular cAMP concentration is associated with the expression of hyperactivated motility (White and Aithen, 1989). Cyclic AMP and Ca^{2+} seems to regulate spermatozoa motility *via* protein phosphorylation. A line of evidence indicates that protein tyrosine phosphorylation is associated with spermatozoa motility and capacitation (Hayashi *et al*., 1987; Visconti *et al* 1995; Burks *et al*., 1995). Although there are many reports suggesting that protein phosphorylation is involved in the regulation of spermatozoa motility, no phosphorylated protein that is associated with mechanism for hyperactivation has been identified.

In Chapter 1, to clarify the precise characteristics of hyperactivation, I examined the time dependent changes during the process of hyperactivation in *in vitro* culture. First, I examined the characteristics of motility pattern with time. Second, to clarify the role of hyperactivation in fertilization, I examined the motility of spermatozoa in the viscoelastic medium that mimics the physiological environment at fertilization. In addition to these analyses, I examined the time dependent changes of protein phosphorylation at tyrosine and serine/threonine residues to investigate the relationship between the changes of motility pattern and those of protein

phosphorylation.

Materials and Methods

Media preparation

The medium used for *in vitro* culture of hamster spermatozoa was developed by Suarez (1988) to maximize the occurrence of hyperactivation and minimize the acrosome reaction. The medium consisted of 110 mM NaCl, 5.0 mM KCl, 2.4 mM Ca Cl_2, 0.49 mM $MgCl_2$, 0.36 mM NaH_2PO_4, 24.9 mM $NaHCO_3$, 25 mM HEPES (N-2-hydroxyethyl-piperazine-N-2-ethane sulfonic acid), 6.25 mM lactic acid, 0.125 mM sodium pyruvate, 0.5 mM hypotaurine, 5.0 mM glucose, 12 mg/ml bovine serum albumin (BSA; fatty acid free Fraction V, Sigma Chemical Inc.), 100 U/ml penicillin, and 0.1 mg/ml streptomycin. The pH was adjusted to 7.4 (Aoki *et al*., 1994).

Spermatozoa preparation

Sexually matured male Syrian hamsters (*Mesocricetus auratus*) were raised and maintained in a light-controlled room (12 h light: 12 h dark) at constant temperature (22 ºC ± 1 ºC). They were killed by chloroform inhalation and the cauda epididymis was promptly isolated. After removing blood from the epididymal surface with physiological salt solution, the distal tubules were punctured with an 18-gauge needle in five to ten places, and a mass of spermatozoa squeezed out with forceps into a plastic Petri dish (35 mm x 10 mm) containing 5 ml of the medium pre-warmed to 37 ºC. The spermatozoa were incubated at 37 ºC under 5 % CO_2 in air. All of the procedures described herein were reviewed and approval by the University of Tokyo Institutional Animal Care and Use Committee, and were performed in accordance with the Guiding Principles for the Care and Use of Laboratory Animals.

Sample preparation

An aliquot (14 μl) of spermatozoa suspension were withdrawn to analyze the movement pattern after 10 min and 1, 2, and 4 h of incubation. The suspension was

diluted with medium to give a final concentration of about 2 x 10^6 spermatozoa per ml. A glass slide, coated with 0.5 % (w/v) PVP (Polyvinylpyrrolidone K-90) to minimize the adhesion of spermatozoa to the glass surfaces, was warmed to 37 ºC. The suspension was placed on the glass slide and covered with an 18 mm x 24mm cover slip to make a depth of about 32 μm. As soon as a sample was prepared, photographs were taken for analysis.

Analysis of the pattern of spermatozoa movement

The pattern of movement was analyzed by taking photographs at 30 frames per second with a FASTCAM-Net high speed camera (PHOTRON Ltd., Tokyo) and the images obtained were recorded and analyzed using Movie Ruler (PHOTRON). The analysis was performed using 30 successive frames, and 3 successive frames were used for the analysis of the number of bends. The exposure time was 1/2000 s under a phase-contrast microscope. Motile spermatozoa were distinguished from immotile spermatozoa as those that were located at different positions in successive frames. Motile spermatozoa were selected for analysis at random, whereas immotile spermatozoa were omitted from analysis. In the analysis, the swimming trajectories of spermatozoa were determined by tracing the sequential positions of the head-mid piece junction. The spermatozoa motility parameters determined in this study were: (1) VSL (straight-line velocity), the distance between the first- and last-tracked points divided by the time elapsed; (2) VCL (curvilinear velocity), the sum of the distances between adjacent points divided by the time elapsed; (3) VAP (average path velocity), a smoothing path of the average of five successive points divided by the time elapsed, which reduced the effect of lateral head displacement (Fig. 1-1); (4) LIN (linearity), an index of the straightness of the pass, given by VSL/VCL; (5) STR (straightness), an index of departure of the spermatozoa path from a straight line, given by VSL/VAP; (6) ALH (amplitude of lateral head displacement), an index of lateral head displacement, given by the maximum value of the distance of any point on the track from the

corresponding the average path, multiplied by two; (7) beat cross frequency, an index of vigor, given by the frequency with which the cell track crosses the smoothing path were determined in the measurement of VCL and VAP, respectively (Cancel *et al*., 2000); and (8) average wavelength, an index of wavelength, derived from the length of the flagellum (180 μm; Woolley, 1977) divided by the number of bends.

Analysis for motility pattern within viscoelastic medium

Spermatozoa were dispersed into the medium, and then pass through a column containing glass beads to prepare samples with high percentages of motile spermatozoa (Mcgrath *et al*., 1977). The column consisted of a Pasteur pipette that had had all but 1.0 cm of the stem removed. One 4.7-5.6 mm glass bead was placed at the base of the column and 1.5 g of 0.18-0.25 mm glass beads (Toshinriko Inc., Tokyo) were packed above the layer bead. These glass beads were prewashed with 6 vol of 1 N HCl, and immediately rinsed thoroughly with double-distilled water. The beads were dried for 2 h in a drying oven at 115 ºC. After drawing the suspension was added into the column several times, 0.5 ml spermatozoa suspension was added to the column, followed immediately by 0.8 ml of the medium to elute the motile spermatozoa. The first eluate (0.3 ml) was discarded and the second eluate (0.5 ml) was collected. The suspension was diluted with the medium to give a final concentration of 2 x 10^6 spermatozoa per ml. Viscoelastic medium was prepared by dissolving polyacrylamide (10,000 kDa, Scientific Polymer Products Inc., Ontario, NY) in the medium to make the concentrations of 16 % (Suarez *et al*., 1992). The suspension was added with the equal volume of viscoelastic medium to the final concentration of 8 %.

SDS-PAGE and Immunoblotting

After various periods of incubation, each 200 μl of the spermatozoa suspension was centrifuged at 3,000 xg for 5 min and the pellets were added with 80 μl of extraction buffer, consisted of 50 mM Tris-HCl, 150 mM NaCl, 1 % Nonidet P-40, 0.5

mM EDTA, 100 μM sodium orthovanadate, 0.1 % SDS, 1 mM DTT, 1 μg/ml aprotinin, 2 μg/ml leupeptin, 1 μg/ml pepstatin, and 100 μg/ml phenylmethylsulfonyl fluoride (pH 8.0), and freezed at –20 ºC. After thawed, the suspensions were centrifuged at 15,000 xg for 5 min at 4 ºC. The supernatants and pellets were denatured for SDS-PAGE as follows. The suspensions were added with the equal volume of x2 SDS sample buffer (Laemmli, 1970) and boiled for 1 min. The pellets was added with 80 μl of extraction buffer, 50 μl of x4 SDS sample buffer and 96 mg of urea and boiled for 1 min. These samples were subjected to electrophoresis on 10 % SDS-PAGE gels. The proteins were electroblotted to a polyvinylidene difluoride membrane (Millipore Corp., Bedford, MA). Non-specific binding sites on the membrane were blocked with 5 % BSA in Tris-buffered saline (TTBS; 150 mM NaCl, 20 mM Tris-HCl, and 0.1 % Tween 20, pH 7.6) for 1 h at room temperature. The blot were kept overnight at 4 ºC with monoclonal anti-phosphotyrosine antibody PY20 (2 μg/ml in TTBS). The blot was then washed with TTBS three times for 10 min each and kept 1 h at room temperature with horseradish peroxidase-conjugated sheep anti-mouse IgG at 1:1000 dilution. After 1 h at room temperature, the membrane was washed with TTBS three times, 20 min each, and the peroxidase activity was detected by using LAS-1000plus (Fuji Photo Film Co. Ltd., Tokyo) and the images obtained were recorded using Image Gauge (Fuji Photo Film Co. Ltd., Tokyo).

Intact spermatozoa phosphorylation

Spermatozoa were incubated with [^{32}P]orthophosphate and the phosphorylation of proteins was traced in the intact spermatozoa using metabolically produced [^{32}P]ATP. After various periods of incubation at 37 ºC with the medium, an equal volume of medium containing 59.2 MBq/ml [^{32}P]orthophosphate (Perkin Elmer Japan Co. Ltd., Tokyo) was added to the spermatozoa suspension and incubated for 20 min. Then, the spermatozoa suspension was centrifuged at 3,000 xg for 5 min at 4 ºC. The pellets were resuspended in 50 μl of extraction buffer, and frozen at –20 ºC for 30 min. After thawing,

the suspensions were centrifuged at 15,000 xg for 5 min at 4 ºC. The supernatants and pellets were denatured for SDS-PAGE as follows. An equal volume of x2 SDS sample buffer was added to the supernatants and boiled for 1 min. To the pellets were added 160 μl of extraction buffer. After mixing, 80 μl of the suspension were added to 50 μl of x4 SDS sample buffer and 96 mg of urea and boiled for 1 min. These samples were electrophoresed on 10 % SDS-PAGE gels. The gels were stained with Coomassie Stain Solution (BIO-RAD Laboratories, CA) for 20 min and destained overnight with 10 % acetic acid and 40 % methanol. They were then dried for 2 h at 80 ºC. The proteins that incorporated ^{32}P were detected using BAS (Fuji Photo Film Co. Ltd.) and the images obtained were recorded using Image Gauge (Fuji Photo Film Co. Ltd.). The intensities of bands on the image were measured using Image Gauge.

To differentiate the proteins phosphorylated at tyrosine residues from those phosphorylated at serine/threonine residues, the gel was subjected to alkali treatment, which removes the phosphorus at serine/threonine residues (Cheng *et al*., 1981; Haystead *et al*., 1990; Cooper *et al*., 1981). After destaining with the dye, the gel was treated with 1 N NaOH for 15 min at room temperature, and then for 1 h at 40 ºC. After treatment with 10 % acetic acid and 40 % methanol for 2 h at room temperature, the gel was kept for 20 min at room temperature with H_2O and dried.

Results

Analysis of the movement pattern with time

The changes in motility pattern before hyperactivation were clarified by analyzing the change in the movement pattern after incubation for 10 min, the spermatozoa swam in a plane without rolling and followed a circular trajectory, in which the hooks of the heads were always directed into the circles. The circular trajectory became much smaller with time until 4 h (Fig. 1-2). The track of lateral movement also increased in length with time. These characteristics of the changes in movement pattern were also shown quantitatively by measuring the parameters VSL, VCL, VAP, LIN, STR, and ALH (Fig. 1-3) and beat cross frequency and average wavelength (Fig. 1-4). VCL, an index of swimming speed, increased slightly until 2 h, and then increased markedly between 2 and 4 h (Fig. 1-3b). VAP, obtained by measuring the smooth path of the average of five successive points to reduce the effect of lateral head displacement, also increased slightly but not significantly until 2 h and then increased markedly between 2 and 4 h (Fig. 1-3c). LIN, an index of path straightness, decreased with time, reflecting the time-dependent decrease in the radium of the circular swimming path or the increase in lateral head displacement (Fig. 1-3d). STR, which is an index of path straightness that excludes the effect of lateral head displacement, decreased markedly between 1 and 2 h, and between 2 and 4 h, indicating that the swimming path became smaller in two steps (Fig. 1-3e). ALH, an index of lateral head displacement, gradually increased with time, reflecting the time-dependent increase in lateral head displacement (Fig. 1-3f).

Measuring beat cross frequency and wavelength with time

The beat cross frequency decreased markedly between 10 min and 1 h, and slightly between 1 and 2 h. It did not change between 2 and 4 h (Fig. 1-4a). In contrast, the wavelength increased with time (Fig. 1-4b); it increased between 10 min and 1 h,

slightly but not significantly between 1 and 2 h, and then markedly between 2 and 4 h.

Analysis for the movement in viscoelastic medium with time

The motility in the viscoelastic medium was analyzed (Fig. 1-5). In the medium with 8 % polyacrylamide, 80 % of spermatozoa were motile, but no spermatozoa showed progressive motion after 10 min of incubation. No spermatozoa swam and most of them: they only vibrated. After incubation for 4 h, a half of spermatozoa swam progressively in 8 % polyacrylamide. Thus, in the viscoelastic medium, the percentages of motile spermatozoa, including vibrating ones, were constantly high (around 80 %), but the percentages of spermatozoa with progressive movement increased after hyperactivation. Thus, spermatozoa seem to increase their ability to swim in the viscoelastic environment with time after starting their movement.

Analysis of protein phosphorylation at tyrosine residues with time

Phosphorylation at tyrosine residues of spermatozoa proteins was examined by immunoblotting with anti-phosphotyrosine antibody. After a 10-min incubation, no tyrosine-phosphorylated protein was detected. However, 75- and 86-kDa proteins were detected in the supernatant of spermatozoa extract after incubation for 1 h. The levels of phosphorylation in these proteins increased with time until 4 h (Fig. 1-6). An 86-kDa protein was also detected in the pellet, but its phosphorylation level did not change with time (data not shown).

Analysis of protein phosphorylation at serine/threonine residues with time

Phosphorylation at serine/threonine residues of spermatozoa protein was examined by incubation with [^{32}P]orthophosphate. One major phosphorylated protein of 41 kDa was detected in the supernatant of spermatozoa extract. The level of phosphorylation in this protein increased between 10 min and 1 h and then decreased

between 2 and 4 h (Fig. 1-7). This protein appeared to be phosphorylated at serine/threonine residue(s), since it disappeared after the alkali treatment. A 41-kDa protein was also detected in the pellet. Its phosphorylation level also changed in the similar manner to that in supernatants, but such a change was not significant (data not shown).

Discussion

Temporal examinations revealed that the parameters used to quantify movement pattern changed in a complex manner. Some parameters changed gradually with time, whereas others changed abruptly before the onset of hyperactivation. Based on microscopic observations, Yanagimachi (1970) reported that hyperactivation occurred abruptly between 2 and 4 h of incubation. Other reports have described hyperactivated spermatozoa as exhibiting a movement pattern alternating between hyperactive and non-hyperactive phases (Johnson *et al*., 1981; Tessler and Olds-Clarke, 1985). These observations indicate that hyperactivation is regulated by an on–off switching mechanism (Ho and Suarez, 2001). In the present study, some movement parameters changed abruptly at the onset of hyperactivation, consistent with previous descriptions. VCL, VAP and STR increased abruptly between 2 and 4 h. However LIN, ALH, beat cross frequency and average wavelength changed gradually with time. These results indicate that complex physiological changes occur before hyperactivation, and that hyperactivation is not controlled simply by an on–off mechanism, but by multiple mechanisms under complex control.

In this study, I found that the level of tyrosine phophorylation gradually increased with time in the 86- and 75-kDa proteins. These proteins would be candidate materials responsible for the gradual change in the motility pattern. The protein of 86 kDa would be identical to the tyrosine-phosphorylated protein of 83 kDa which was previously suggested to be AKAP83 in hamster spermatozoa (Kula Nand *et al*., 2002). This protein may be implicated with the gradual change in the mechanism(s) regulating the path straightness and the lateral head displacement. On the other hand, the candidate material responsible for the abrupt change in the motility pattern is a 41-kDa serine/threonine phophorylated protein, since its phosphorylation level increased between 10 min and 1 h and then decreased between 2 and 4 h. This protein may affect the abrupt changes in the mechanism(s) regulating the path velocity.

The ability of spermatozoa to swim in a viscoelastic medium was enhanced between 2 and 4 h after the onset of hyperactivation. Spermatozoa need to pass through various levels of viscoelastic environments until they reach an oocyte *in vivo*. Viscoelastic environments are composed of mucous secretions in the oviduct, a viscoelastic extracellular cumulus matrix, and the elastic fibrillar network of the zona pellucida (Suarez *et al*., 1992). In this study, I demonstrated that the ability of spermatozoa to swim in a viscoelastic medium was enhanced after the onset of hyperactivation. Although spermatozoa initially could not move progressively and only vibrated, they could swim actively after hyperactivation. These results suggest that the propulsion force for the progressive motility is enhanced after hyperactivation, and that under viscoelastic condition, spermatozoa are not able to move progressively before the force reach a threshold level. This suggests the physiological significance of hyperactivation.

The present study demonstrates that the parameters related to the patterns of movement change in various manners with time before hyperactivation. The results lead to the hypothesis that multiple factors are involved in the regulation of hyperactivation. In addition, the propulsive force for the progressive movement seems to increase in the hyperactivated spermatozoa, since they can swim in a viscoelastic medium and the parameters for swimming speed, *i.e.* VCL and VAP increased.

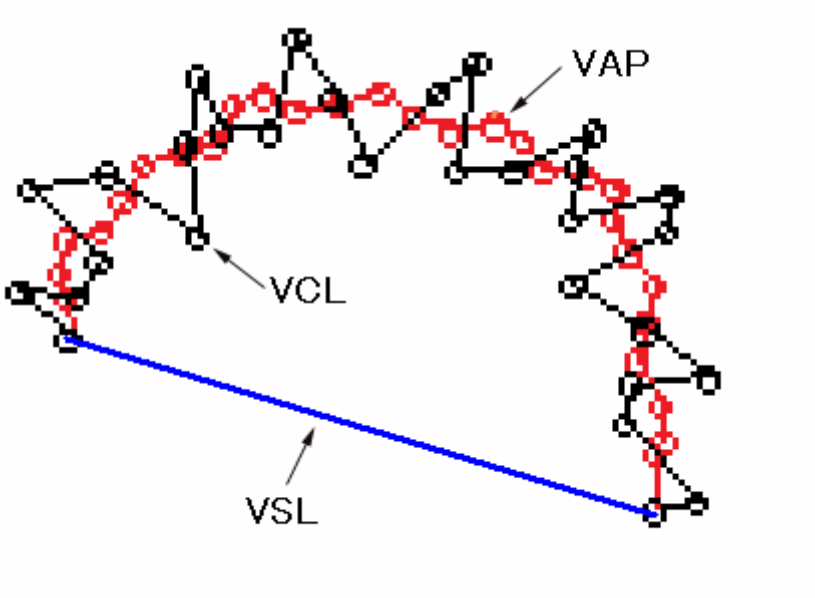

Fig. 1-1. Analysis for movement pattern. The positions of head-midpiece junction were traced to obtain the trajectory of movement from 30 successive of images taken at a rate of 30 frames per second on high speed camera. The straight line velocity (VSL) was determined by measuring the distance between the first and last points of trajectory. The curvilinear velocity (VCL) was determined by measuring the sum of the distances between adjacent points. The average path velocity (VAP) was determined by measuring the sum of the distances between the points connecting the averages of successive 5 points.

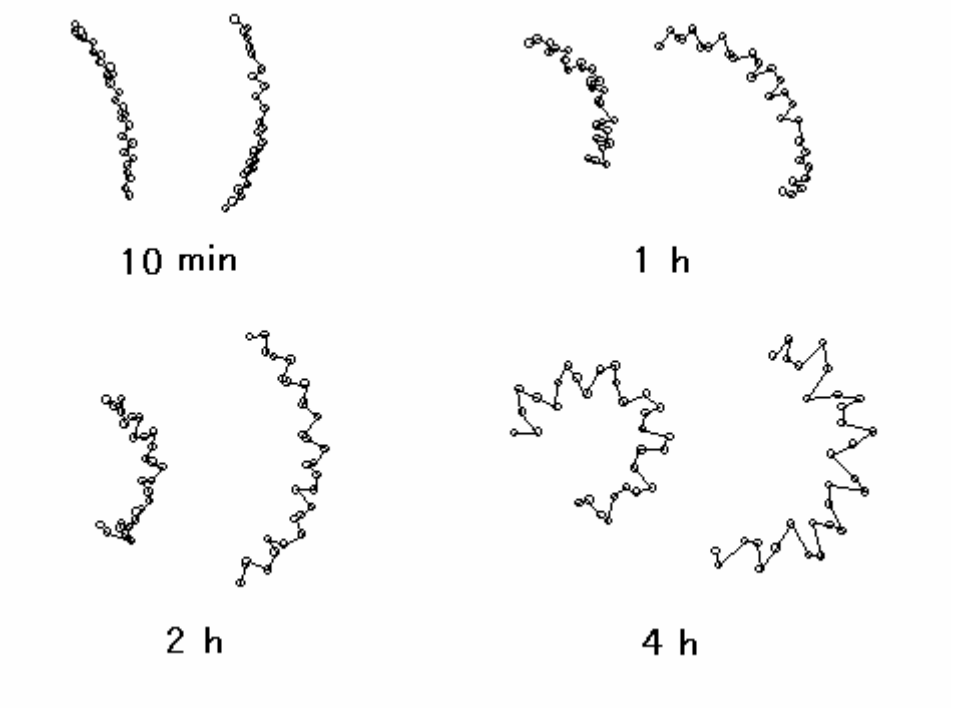

Fig. 1-2. Typical movement trajectories of hamster spermatozoa. Photographs were taken at 30 frames per second. The dots show the location of the head-midpiece junction in 30 successive frames. The spermatozoa were incubated for 10 min and 1, 2, and 4 h.

Fig. 1-3. Analysis of the movement pattern of hamster spermatozoa using various parameters. Photographs were taken at 30 frames per second. The analysis used 30 successive frames. (a) VSL, straight-line velocity. (b) VCL, curvilinear velocity. (c) VAP, average path velocity. (d) LIN, linearity. (e) STR, straightness. (f) ALH, amplitude of lateral head displacement. These parameters are described in the *Materials and Methods*. The experiments were repeated three times. The data were pooled and are expressed as the mean ± S.E.M. (n = 18). Asterisks indicate significant differences from the value at the previous time point (Student's *t*-test; **: $P < 0.01$ and *: $P < 0.05$).

(a)

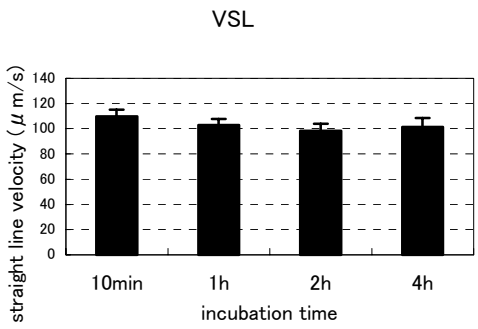
VSL
straight line velocity (μm/s)
140
120
100
80
60
40
20
0
10min
1h
2h
4h
incubation time

(b)

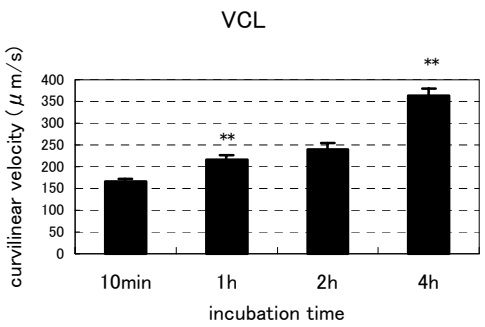
VCL
curvilinear velocity (μm/s)
400
350
300
250
200
150
100
50
0
**
**
10min
1h
2h
4h
incubation time

(c)

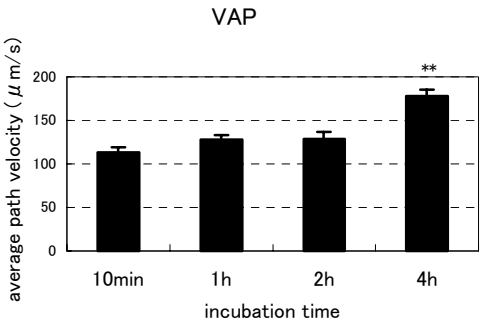
VAP
average path velocity (μm/s)
200
150
100
50
0
**
10min
1h
2h
4h
incubation time

(d)

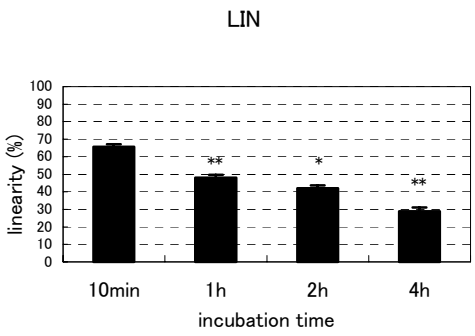
LIN
linearity (%)
100
90
80
70
60
50
40
30
20
10
0
**
*
**
10min
1h
2h
4h
incubation time

(e)

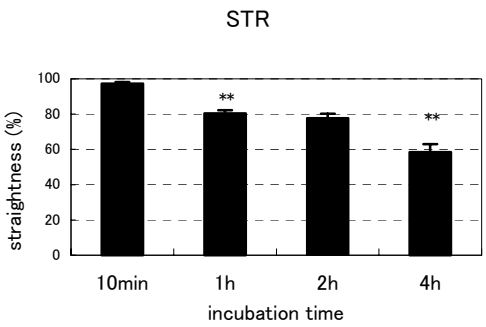
STR
straightness (%)
100
80
60
40
20
0
**
**
10min
1h
2h
4h
incubation time

(f)

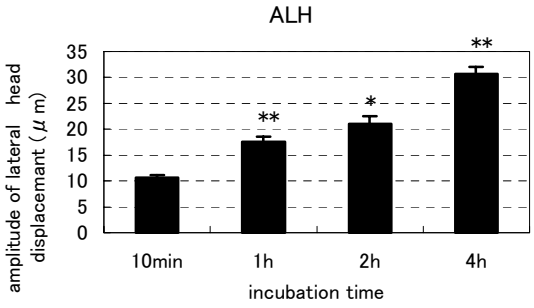
ALH
amplitude of lateral head displacemant (μm)
35
30
25
20
15
10
5
0
**
**
*
10min
1h
2h
4h
incubation time

(a)

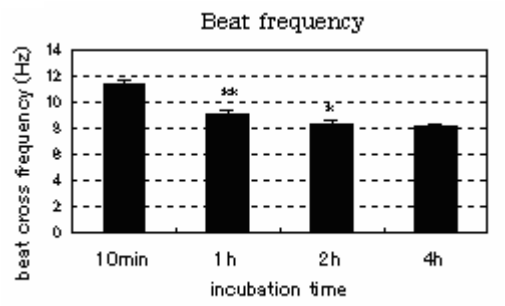

(b)

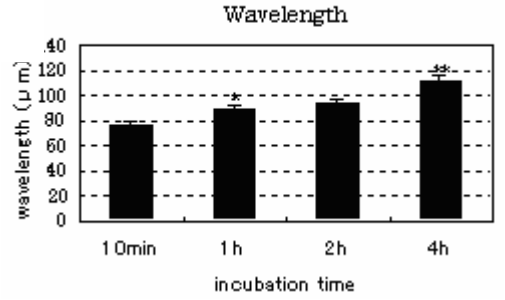

Fig. 1-4. Analysis for beat frequency and average wavelength. Photographs were taken in 30 frames per second. The analysis was performed using successive 30 frames. (a) beat frequency. (b) average wavelength. Details of these parameters are described under *Materials and Methods*. The experiment was conducted three times and in each experiment, six spermatozoa were analyzed. The data were accumulated and expressed as the mean ± S.E.M. (n=18). Asterisks represent the significant differences from the values of previous time points (by Student's t test; ＊＊: $P < 0.01$ and ＊: $P < 0.05$).

Fig. 1-5. Analysis for motility pattern in a viscoelastic medium. Spermatozoa were incubated in the medium with 0 % and 8 % polyacrylamide (PAA). Photographs were taken in 30 frames per second. The analysis was performed using successive 30 frames. (a) percentages of motile spermatozoa. (b) percentages of spermatozoa with movement at the speed more than 10 μm/s. The spermatozoa were passed through a column containing glass beads to obtain samples with high percentages of motile spermatozoa. The experiments were repeated three times. The data were accumulated and expressed as the percentages of spermatozoa. In all experiments, more than 28 spermatozoa were analyzed.

(a)

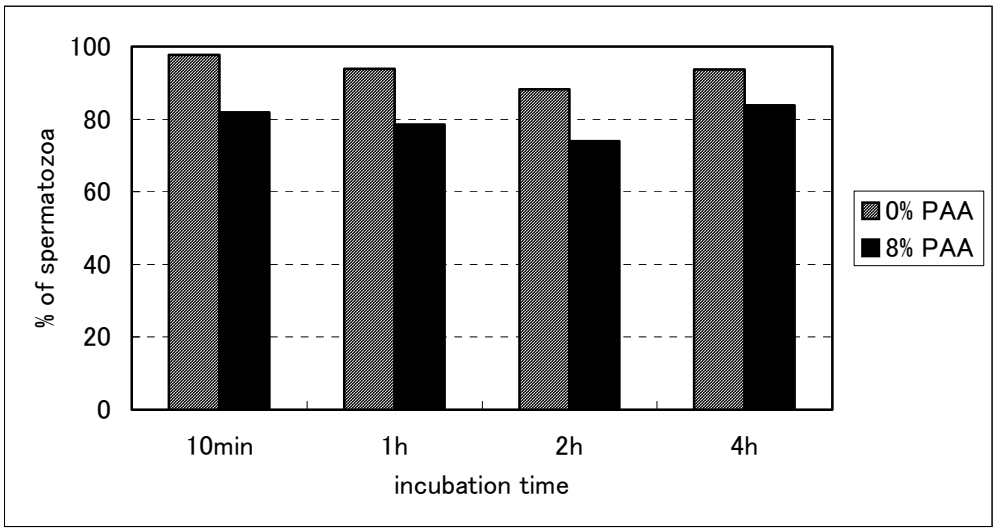
100
80
60
40
20
0
% of spermatozoa
10min
1h
2h
4h
incubation time
0% PAA
8% PAA

(b)

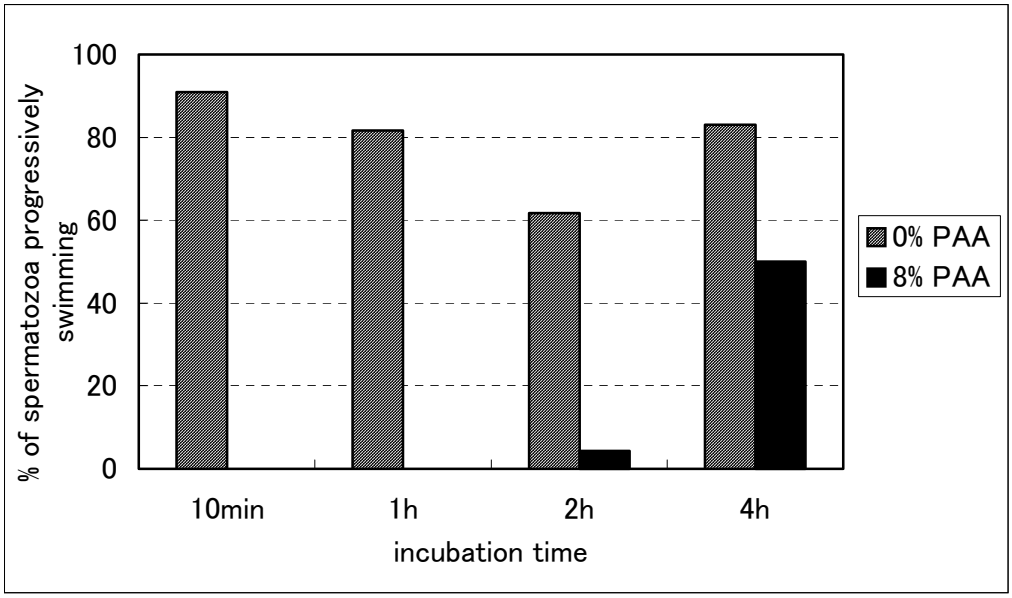
100
80
60
40
20
0
% of spermatozoa progressively swimming
10min
1h
2h
4h
incubation time
0% PAA
8% PAA

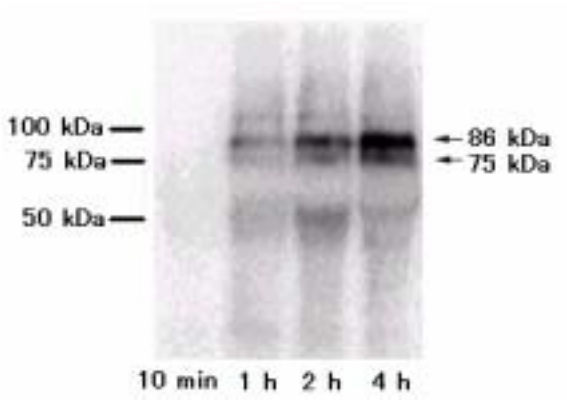

Fig. 1-6. Analysis of protein tyrosine phosphorylation. Spermatozoa were lysed in extraction buffer and centrifuged to obtain the supernatant fraction after incubation for 10 min, 1 h, 2 h, and 4 h. The spermatozoa proteins were separated on SDS-PAGE and probed with anti-phosphotyrosine antibody PY-20. Molecular mass standards are indicated to the left of the lanes.

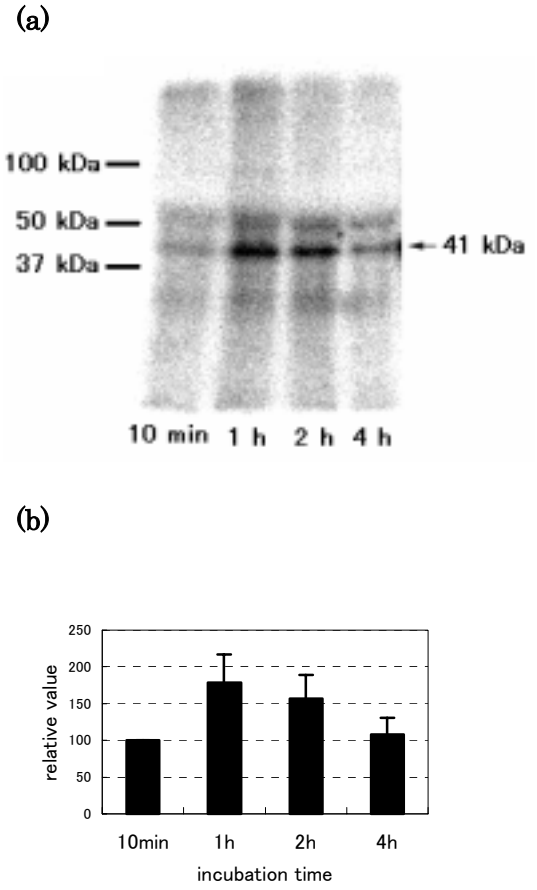

Fig. 1-7. Analysis of phosphoproteins incorporating ^{32}P. (a) An image of phosphorylated proteins after SDS-PAGE. Ten minutes before the indicated time of incubation, the spermatozoa suspensions were added to an equal volume of medium containing [^{32}P]orthophosphate and incubated for 20 min. After the incubation, the spermatozoa were lysed in extraction buffer and centrifuged to obtain the supernatant fraction. The spermatozoa proteins were separated on SDS-PAGE and the proteins incorporating ^{32}P detected using BAS (Fuji Photo Film Co. Ltd.). Molecular mass standards are indicated to the left of the lanes. (b) The level of phosphorylation of the 41-kDa protein. The phosphorylation level was examined by measuring the intensity of the band at 41 kDa for each incubation time. The value at 10 min was set as 100 % for relative evaluation. The experiments were conducted five times. The bars represent the S.E.M.

Chapter 2

Analysis of flagellar bending in hyperactivated hamster spermatozoa

Abstract

In chapter 1, I showed the characteristics of movement in hyperactivated spermatozoa by the quantitative analyses for the movement pattern. Since the propulsive force for the movement of spermatozoa is generated by flagellar bending, the analysis of flagellar bending is important in understanding the mechanism regulating the movement of spermatozoa. In this chapter, to analyze flagellar bending, the bend angles were measured after dividing the images of flagellum into short lengths. Flagellar bending changed in different manners in each region during incubation. The asymmetry in the direction of the curve of the head gradually increased with time in the first half of the flagellum. The flexibility, which was determined by measuring the amplitude of the bending and the rate of the change in bend angles, abruptly decreased between 10 min and 1 h, and then increased between 2 and 4 h in the first half of flagellum. These results indicate that multiple factors are involved in the regulation of hyperactivation. In the analysis for the propagation of wave, I found that the large wave which occurred in the basal region is propagated to the distal region both in the hyperactivated and non-hyperactivated spermatozoa incubated for 10 min and 4 h, respectively. However, the additional small waves which occurred in the mid region were propagated to the distal region in the non-hyperactivated spermatozoa but not hyperactivated ones. This result suggests that the additional small waves interfere in the formation of complete cycle of the large waves to reduce the propulsive force in the swimming of non-hyperactivated spermatozoa and that the absence of the additional small wave contribute to the formation of complete cycle of the waves in the hyperactivated spermatozoa. Finally, in the analysis for the bending rate, the propulsive force was calculated on each position along with whole flagellum. By this analysis, I identified the effective stroke in the flagellar bending. The spermatozoa alternately produce the effective and ineffective stroke for the progressive movement. When the effective stroke generates the propulsive force, the high amplitude would be an important determinant

for generating the large propulsive force. Therefore, the hyperactivated spermatozoa generate larger propulsive force, since they bend their flagellum with higher amplitude than non-hyperactivated ones.

Introduction

Flagellar bending is generated by the sliding of adjacent doublet microtubules *via* the activity of dynein arm ATPase (Shingyoji *et al*., 1977). Dynein arms are oscillating force generators and they may be involved in the basal mechanism of cyclical flagellar beating (Shingyoji *et al*., 1998). The flagellar beating consists of an undulating wave that propagates from base to tip. According to the Newton's Third Law of Motion (Law of Conservation of Momentum), a force equal in magnitude and opposite in direction to the tip will push the spermatozoa forward (Jahn and Votta, 1972). However, it is not clear how flagellar bending and their cyclical propagation convert into the motility in spermatozoa.

Hyperactivated spermatozoa is a good model for the investigation of the mechanism by which flagellar bending generate the motility of spermatozoa. In chapter 1, I clarified the characteristics in the movement pattern of hyperactivated spermatozoa. The main differences between hyperactivated spermatozoa and non-hyperactivated ones are loss of path straightness and increase in the propulsive force. Since these differences would be generated by the differences in the mechanisms regulating flagellar bending and generating the propulsive force, it is useful for understanding those mechanisms to compare the patterns of flagellar bending between hyperactivated and non-hyperactivated spermatozoa. However, most analyses in the previous studies, *e.g.* the CASA analysis, have measured only parameters involved in the movement patterns, and not flagellar bending.

In chapter 2, to clarify the mechanism by which flagellar bending efficiently generates propulsive force in spermatozoa, I examine the change in flagellar bending during the process of hyperactivation. First, I examine the change in flagellar bending with time. Second, to clarify the mechanism of hyperactivation from the aspect of flagellar bending, the bending rate and the propagation of waves were examined.

Materials and Methods

Preparation for media and spermatozoa sample

The media and spermatozoa samples were prepared as described in chapter 1.

Analysis for flagellar bending

Flagellar bending of spermatozoa was analyzed by taking photographs at 250 frames per second with a FASTCAM-Net high-speed camera (PHOTRON). The images obtained were recorded and analyzed by using Movie Ruler (PHOTRON) using flagellar image analysis software, Bohboh (BohbohSoft, Tokyo). In the analysis using Movie Ruler, was performed using 8 successive frames at every 3 frames were used, and 120 successive frames were used for the analysis of the bending rate and the propagation of waves. The exposure time was 1/2000 s under a phase-contrast microscope. The direction of each bend was determined according to the direction of hook-shaped projection of head as described by Woolley (1977). A bend in the same direction as the curve of the hook-shaped head was defined as a reverse bend (R-bend) and one in the opposite direction was defined as a principal bend (P-bend). Reverse bends were assigned a plus value and principal bends a minus value (Fig. 2-1a). To measure regional bend angles in the flagellum, each image of a flagellum was divided into 30 μm sections from the head-midpiece junction. The points that were 0, 30, 60, 90, 120, and 150 μm from the head-midpiece junction were termed points O, A, B, C, D, and E, respectively (Fig. 2-1b). The length of midpiece region is 51 μm and the region corresponds to region O-A. Tangent lines were drawn at each point. The regional bend angle was measured as the supplementary angle formed by two successive tangents. The angles between the tangent lines to O and A, A and B, B and C, C and D, and D and E were termed θ_A, θ_B, θ_C, θ_D, and θ_E, respectively (Fig. 2-1c). In 8 successive frames, the maximum and minimum of each regional bend angle, the difference between the maximum and minimum, the average of the maximum and minimum, and sum of θ_A-θ_E

were determined. In addition, the rate of change of falgellar bending was examined by determining the changes in each regional bend angle between two successive frames.

Procedure for calculation of the propulsive force

The propulsive force in flagellum was calculated using the method by Gray and Hancock (1955). The motion at a low Reynolds number such as the propulsion in spermatozoa is regarded as directly proportional to the velocity of displacement and to the viscosity of the medium. Therefore, the propulsive forces exerted on a short element (δs) in the flagellum are represented as these values. The net propulsive force (dF) is

$$dF = \left[(C_N - C_T)\, V_y \sin\theta\cos\theta - V_x (C_N \sin^2\theta + C_T \cos^2\theta) \right] \delta s$$

The velocity from the longitudinal displacement (Vx) and the transverse displacement (Vy) is

$$V_x = (X_{K+1} - X_K)\, f$$
$$V_y = (Y_{K+1} - Y_K)\, f$$

where X = X coordinate, Y = Y coordinate, k = frame number, and f = frame rate (Hz). The coefficients of resistance acting tangentially (C_T) and normally (C_N) to the surface of the element for a medium of known viscosity is

$$C_T = -\frac{2\pi\mu}{(\ln\frac{d}{2\lambda}) + 0.5}$$
$$C_N = 2\,C_T$$

where μ = the viscosity of the medium, d = the radius of the flagellum, and λ = the wavelength. C_N is effectively twice C_T for very thin filaments such as the flagellum (Hancock, 1953). The values measured in chapter 1 were assigned to these valuables.

Results

Temporal change in the pattern of flagellar bending

Typical patterns of flagellar bending are shown in Fig. 2-2 by tracing the movement of the flagellum in the spermatozoa whose heads' positions are fixed. As spermatozoa were incubated in the medium longer time, the amplitude and asymmetry of flagellar bending appeared to increase.

Changes in flagellar bending were precisely analyzed by measuring the bend angles in different regions, as the bending would change in different manners in each region during incubation. The changes in the average bend angles for each region O-A through to D-E (θ_A-θ_E) (Fig. 2-3a), show that in all regions, the values increased between 10 min and 1 h, indicating an increase in the asymmetry of the direction of the R-bend during this period. The values of θ_A, θ_B, and θ_C gradually increased with time until 4 h, indicating that the asymmetry of the direction of the R-bend increased continuously in the first half of the flagellum. The value of θ_B in region A-B, the region generating the dominant second bend, increased markedly between 2 and 4 h. However, θ_E increased between 10 min and 1 h and then decreased until 4 h. Thus, the bend angles in each region changed differently. The bend angles in all regions were summed to analyze the total change in the asymmetry of bending in the entire flagellum. The sum of θ_A-θ_E increased markedly between 10 min and 1 h and then increased gradually, but not significantly, until 4 h (Fig. 2-3b).

The maximum and minimum bend angles in 8 successive frames in each region were determined. Asymmetry can be evaluated from these values, as well as from the average bend angles discussed above. In addition, these values allow evaluation of changes in flexibility. The maximum values decreased between 10 min and 1 h and then increased until 4 h in all regions of the flagellum except for the distal region, D-E (Fig. 2-4a). The changes in the minimum values were almost the reverse of those in the maximum values. The maximum and minimum values were averaged in each region to

evaluate the asymmetry (Fig. 2-4b). The pattern of change in these values was similar to that in the average bend angles described above (Figs. 2-3a and 2-4b); the average of maximum and minimum values gradually increased with time in the first half of the flagellum. The flexibility was evaluated using the difference between the maximum and minimum values (MX-MN). MX-MN decreased prominently between 10 min and 1 h in all regions. Subsequently, at 4 h, it abruptly increased to near the original value at 10 min in regions O-A, A-B and B-C, but not in regions C-D and D-E, indicating that the flexibility decreased at 1 h in all regions of the flagellum, and then restored at 4 h in the first half of the flagellum, but not in the second half (Fig. 2-4c).

Although the changes in MX-MN reflect changes in flexibility, this index is insufficient for evaluating the flexibility by itself; rather, it reflects amplitude. The flagellum would not appear to be flexible when the movement of the flagellum is slow, even if the amplitude is high. Therefore, the flexibility was evaluated by determining the changes in the bend angles between two successive frames (Fig. 2-5). These values represent the bending rates of flagellum and the velocity of microtubule sliding. The values changed in a manner similar to the change in MX-MN (Figs. 2-4c and 2-5). They decreased at 1 h in all regions and then abruptly increased at 4 h in regions O-A and A-B. In region B-C, the values remained constant between 1 and 4 h, whereas they decreased in regions C-D and D-E. Combined with the value of MX-MN, the flexibility decreased at 1 h in all regions and then was abruptly restored at 4 h in the first half of the flagellum.

Analysis for the propagation of waves - identification of interference waves

Since the bending is propagated on the flagellum as a wave, it is important in clarifying the characteristics of flagellar bending pattern in hyperactivated spermatozoa to analyze the pattern of the propagation of wave. For this analysis, the changes in bend angle in the regions O-A, A-B, B-C, C-D, and D-E were examined by plotting the bend angles with the course of time, which shows the pattern of the propagation of wave (Fig.

2-6). In the spermatozoa incubated for 4 h, waves occurred in a constant rate in all regions on the flagellum, suggesting that a wave which has occurred in the basal region is smoothly propagated to the distal region. However, in the spermatozoa incubated for 10 min, in addition to the large waves which occurred in all regions as observed in the spermatozoa incubated for 4 h, there were also small waves which occurred only in mid- and distal regions (B-C, C-D and D-E) but not the basal regions (O-A or A-B) (Figs. 2-6 and 2-7). These additional small waves appeared between the large waves, and seemed to interfere in the formation of complete cycle of the large waves.

To further clarify the propagation of the waves, I plotted the time point at which the peak of wave appeared (Fig. 2-8). The results show that in the spermatozoa incubated for 10 min, the large waves which had appeared in the basal region (O-A) were propagated to the distal region in order from A-B to D-E. In addition to these large waves, small waves appeared in the mid-region, B-C and were propagated to the distal region. Thus, there are two independent streams of waves propagated on the flagellum in the spermatozoa incubated for 10 min. However, only one stream was observed in the spermatozoa incubated for 4 h. Since the additional small waves interfere in the smooth propagation and the formation of complete cycle of the large wave, the spermatozoa incubated for 4 h, in which no small wave arises, efficiently generate the larger propulsive force than those incubated for 10 min.

Analysis for the bending rate of flagellum – identification of effective stroke in flagellar bending

The trajectory of flagellum was analyzed by tracing the whole flagellum in the freely swimming spermatozoa. Fig. 2-9 shows that the flagellum drew a trajectory which curved to the same direction as the curve of head. Tracing the positions of A-D, it revealed that all positions showed zig-zag trajectory both in the spermatozoa which had been incubated for 10 min and 4 h. When the direction of progression in spermatozoa was defined by the line connecting the outmost points in the arc trajectory of

head-midpiece junction, all the positions went and returned along the line crossing the direction of progression, in which they made no progression, and moved along the innermost line of the trajectory of whole flagellum, in which they made a progression. However, they did not move along the outmost line, indicating that they made no progression on the outmost line of the trajectory. Thus, they made a progression only on the innermost line but not outmost line, drawing asymmetric trajectories, which suggested that the propulsive force is generated asymmetrically in a cycle of flagellar bending. The difference in P- and R-bends would be involved in this asymmetry.

To address this possibility, the bending rate was analyzed, because it is an important factor to determine the propulsive force. In Fig. 2-10, the curvatures at the positions A-D on the flagellum were plotted with the course of time, in which the slope of the line indicates the bending rate. Comparing the slopes between the lines going from the point of maximum value (MX) to that of minimum value (MN), which corresponds to the bending with the direction from R- to P-bend, and those going from the points of MN to MX, which corresponds to the one from P- to R-bend, it revealed that the slope for MX to MN (R to P) was always higher than that for MN to MX (P to R) at all positions of the flagellum in the spermatozoa incubated both for 10 min and 4 h, except for the position A (Figs. 2-10 and 2-11). These results demonstrated that the bending rate is not constant in a cycle of flagellar bending and is higher when the flagellum bends from the direction of P-bend to that of R-bend.

To clarify when the propulsive force is efficiently generated in a cycle of flagellar bending, the propulsive force in each position on the flagellum was calculated by using the formula proposed by Gray and Hancock (1955). Interestingly, the value of propulsive force was positive whenever the flagellum bends from the direction of P-bend to that of R-bend, in which the bending rate was lower, and was zero or rather negative from R- to P-bend, in which the bending rate was higher, at all positions on the flagellum of the spermatozoa incubated for 4 h (Fig. 2-12). In the spermatozoa incubated for 10 min, the similar results were obtained, with some exceptions. These

exceptions would be caused by the interference waves. These results demonstrated that spermatozoa alternately produce the effective and ineffective stroke for the progressive movement.

When the effective stroke generates the propulsive force, the amplitude would be the most important element that determines the propulsive force. The amplitudes of the bending were measured at the positions A-D on the flagellum of the spermatozoa which had been incubated for 10 min and 4 h (Fig. 2-13). The results showed that the amplitude was higher in the spermatozoa incubated for 4 h than those for 10 min in all positions except for position A at which there is no difference. Therefore, the higher amplitude seems to contribute to the larger propulsive force in the hyperactivated hamster spermatozoa.

Discussion

In this chapter, I identified the factors which were involved in the propulsive force by comparing the patterns of flagellar bending between hyperactivated and non-hyperactivated spermatozoa. First, I found that only the effective stroke which is the bending with the direction from P- to R-bend generates a propulsive force. To produce the large effective stroke, the amplitude is an essential determinant. The amplitude was higher in hyperactivated spermatozoa incubated for 4 h than non-hyperactivated spermatozoa incubated for 10 min. Second, the disappearance of additional small waves was important in generating the efficient flagellar bending. In the non-hyperactivated spermatozoa, a small additional wave arose in the mid-region on the flagellum and interfered the accomplishment of complete cycle of the large wave. This additional wave disappeared in hyperactivated spermatozoa. Thus, by investigating the pattern of flagellar bending in hyperactivated spermatozoa, various factors involved in the regulation of the motility of spermatozoa have been clarified.

Analyzing the regional changes in flagellar bending is important for investigating the characteristics of the flagellar bending in hyperactivated spermatozoa, as several reports indicate that regulation of flagellar bending differs regionally in the flagellum. Local iontophoretic application of ATP demonstrated that sliding occurs in each region independently (Singyoji *et al*., 1977). The α subunit of cyclic nucleotide-gated channels is observed along the entire flagellum, whereas the short β subunit is localized in the principal piece of the flagellum (Wiesner *et al*., 1998). CatSper, which is a putative sperm cation channel regulating cAMP-mediated Ca^{2+} influx, is localized in the principal piece of the flagellum (Ren *et al*., 2001). The results in this chapter have demonstrated that the bending pattern changes in a different way in each region during the course of hyperactivation. The degree of asymmetry of the direction of the R-bend increased in the first half of the flagellum with time, but not in the second half. It increased markedly between 2 and 4 h in region A-B (Figs. 2-3a and

2-4b). The pattern of change corresponded to changes in the movement pattern. The trajectory of movement became smaller with time and especially much smaller between 2 and 4 h (Fig. 1-2 in chapter 1). In contrast, when the bend angles of all the regions were summed, the asymmetry increased prominently between 10 min and 1 h (Fig. 2-3b). Therefore, the changes in movement pattern seem to reflect those of the bending in the first part of the flagellum, but not in the second part. This is plausible because the second bend, which is the dominant bend, occurs in the first half of the flagellum and frequently in region A-B. These results indicate that the regulation of asymmetry differs in parts of the flagellum, and that the increase in the angle of the dominant bend in the direction of the R-bend affects the movement pattern of hyperactivated spermatozoa.

The differences of regional changes in flagellar bending may be affected by the difference in the cytoskeletal structures between midpiece and principal piece. It is estimated that region O-A lies in the midpiece and regions B-C, C-D, and D-E lie in the principal piece, as the lengths of midpiece and principal piece are 51 and 126 μm, respectively (Woolley, 1977). The flexibility, evaluated by changes in the bend angles between two successive frames, changed in a similar manner among regions B-C, C-D, and D-E: it decreased with time. However, flexibility changes in a different manner in region O-A and A-B from others: it decreased at first, and then increased. In addition, the additional waves were observed only regions B-C, C-D, and D-E in 10 min incubated spermatozoa. The major structural difference between the midpiece and principal piece is that only the principal piece is wrapped by fibrous sheath (Woolley, 1977; Si and Okuno., 1993; Carrera *et al*., 1994; Moss *et al*., 1999; Kula Nand and Shivaji, 2002). The structural differences change like the regional stiffness. Thus, the difference may affect the flexibility of the flagellum and the additional waves propagating in the flagellum.

Hyperactivation has not been defined using quantitative measurements of flagellar bending. Although many studies have measured several parameters, they have showed only that the values of the parameters changed after hyperactivation occurred

(Ho and Suarez, 2001). Furthermore, few reports explain how to changes in such parameters are responsible for the changes in motility with hyperactivation. In this chapter, the change in various parameters was measured with time, and it was determined that the parameters changed in various manners. From microscopic observations, however, hyperactivation appeared to occur abruptly (Yanagimachi, 1970). Two parameters of flagellar bending should be considered to explain which parameters are related to hyperactivaion and how the changes in such parameters are responsible for the change to hyperactivated movement. First, the asymmetry of the direction of the R-bend gradually increased in the first half of flagellum with time (Fig. 2-3 and 2-4b). Second, flexibility abruptly decreased between 10 min and 1 h and abruptly increased between 2 and 4 h (Fig. 2-4c, and 2-5). As it has been reported that hyperactive motility involves asymmetric movement and an elastic flagellum (Ho and Suarez, 2001), it is postulated that the synergic effects of the increase in asymmetry and flexibility at between 2 and 4 h give the impression of an abrupt change in motility pattern.

I have identified the bending with the direction from P- to R-bend as the effective stroke (Fig. 2-12). It was previously suggested that the bundle of microtubule doublets 4-5-6-7 are located on the same side as the curve of the hook-shaped head and the bundle of 9-1-2 microtubules on the opposite side (Lindemann *et al*., 1992; Si and Okuno, 1995). Considering that the dynein arm attatched to the doublet microtubule (n) pushes the next doublet (n+1) to the direction from base to tip (Sale and Satir, 1977), the dynein arms attached to 4-5-6-7 microtubules would generate the effective stroke for propulsive force. In the ‘switch-point’ hypothesis, advocated by Satir (Satir, 1985; Holwill and Satir 1994), the active bundles of the dynein arms switch in an alternating fashion, which generates alternating bending between P- and R-bend. These reports suggest that the dynein arms attached to microtubules 4-5-6-7 and 9-1-2 might be important in generating the effective and ineffective stroke, respectively. In accordance with the flagellar bending of hamster spermatozoa, the ciliary beat also consists of asymmetrical two components, the power stroke and return stroke (Jahn and Votta,

1972). Cilium has the same axoneme structure which consists of 9+2 arrangement of microtubule as flagellum. Although it has not been currently determined which doublets of microtubule generate power stroke, it would be interesting if they correspond to those for effective stroke in the flagellum of hamster spermatozoa.

To generate the large propulsive force, the amplitude is an important factor in the flagellar bending. The hyperactivated spermatozoa generate larger propulsive force than non-hyperactivated ones (Figs.1-3b and 1-5 in chapter 1), and they bend their flagellum with higher amplitude (Fig. 2-13). The decrease in beat frequency would be the major contributor to this high amplitude in hyperactivated spermatozoa: the beat frequency decreased in the hyperactivated spermatozoa after 4 h of incubation (Fig. 1-4a in chapter 1). The higher amplitude is generated when microtubules slide to more distant part of the flagellum. Since the bending rate was not increased in hyperactivated spermatozoa after 4 h of incubation (Fig. 2-11), microtubules should continue to slide to one direction for a long time to slide a long distance. Thus, the time cycle per a stroke is longer in hyperactivated spermatozoa than in non-hyperactivated ones to allow the microtubules slide to a longer distance, which results in the larger amplitude. In addition, I found that additional small waves arose in the non-hyperactivated spermatozoa but not in hyperactivated ones (Figs. 2-7 and 2-8). These additional waves would decrease the amplitude. The additional waves interfere in the smooth propagation and disturb the formation of complete cycle of the large wave, which would reduce the amplitude in flagellar bending. The disappearance of the small additional waves would contribute to the increase of amplitude in the hyperactivated spermatozoa.

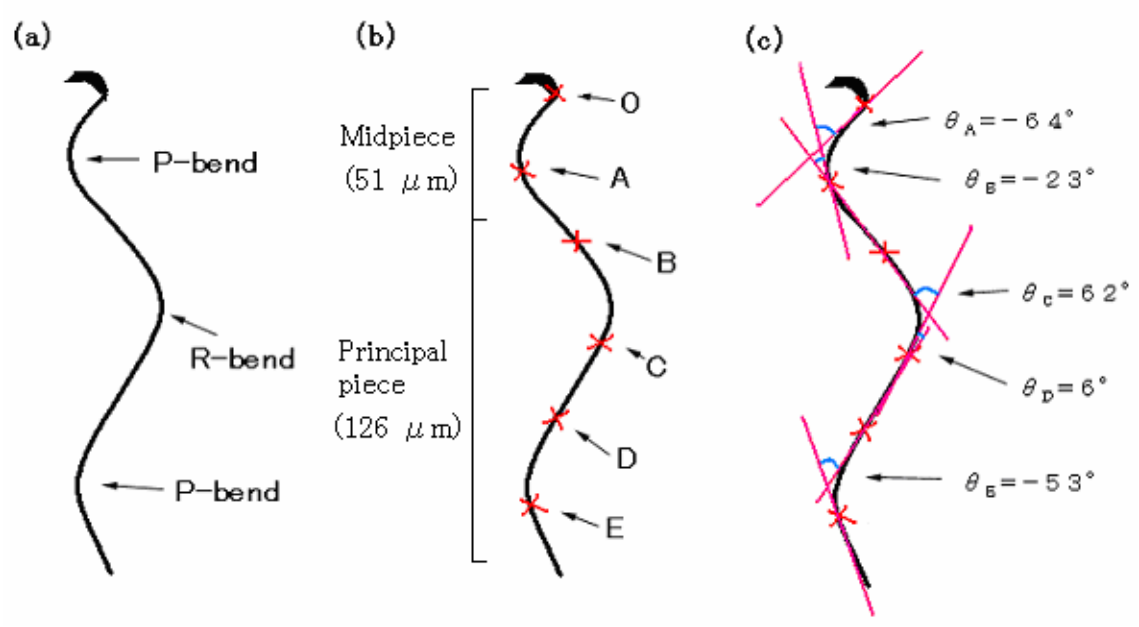

Fig. 2-1. Procedure used to analyze flagellar bending in hamster spermatozoa. (a) Bends in the same direction as the curve of the hook-shaped head were defined as reverse bends (R-bends) and those in the opposite direction as principal bends (P-bends). (b) The points on the flagellum 30, 60, 90, 120, and 150 μm from the head-midpiece junction (O) were designated as A, B, C, D, and E, respectively. The lengths of midpiece and principal piece are 51 and 126 μm, respectively. (c) The bend angles were measured as the angles between consecutive tangents. The regional angles between O and A, A and B, B and C, C and D, and D and E were termed θ_A, θ_B, θ_C, θ_D, and θ_E, respectively. R-bends were assigned plus values and P-bends were assigned minus values.

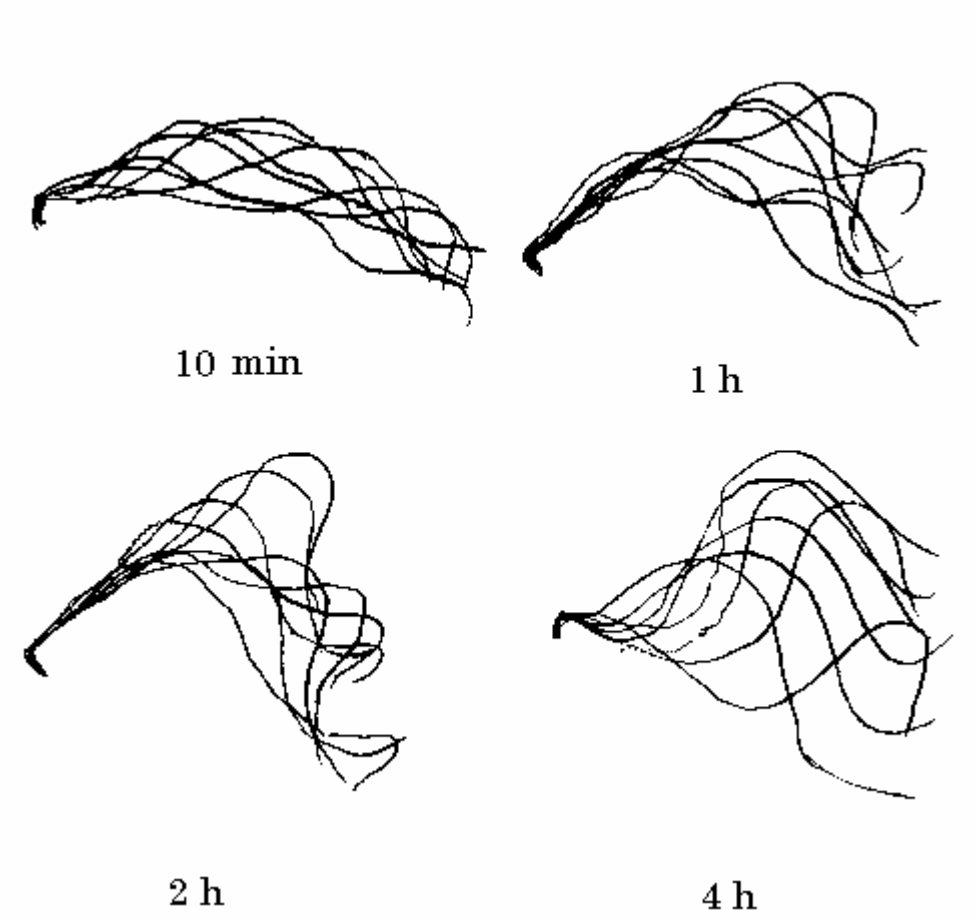

Fig. 2-2. Typical patterns of flagellar bending. Photographs were taken at 250 frames per 3 seconds. Images of spermatozoa were traced in 8 successive frames after superimposing the axes of the heads. The spermatozoa were incubated for 10 min, and 1, 2, and 4 h.

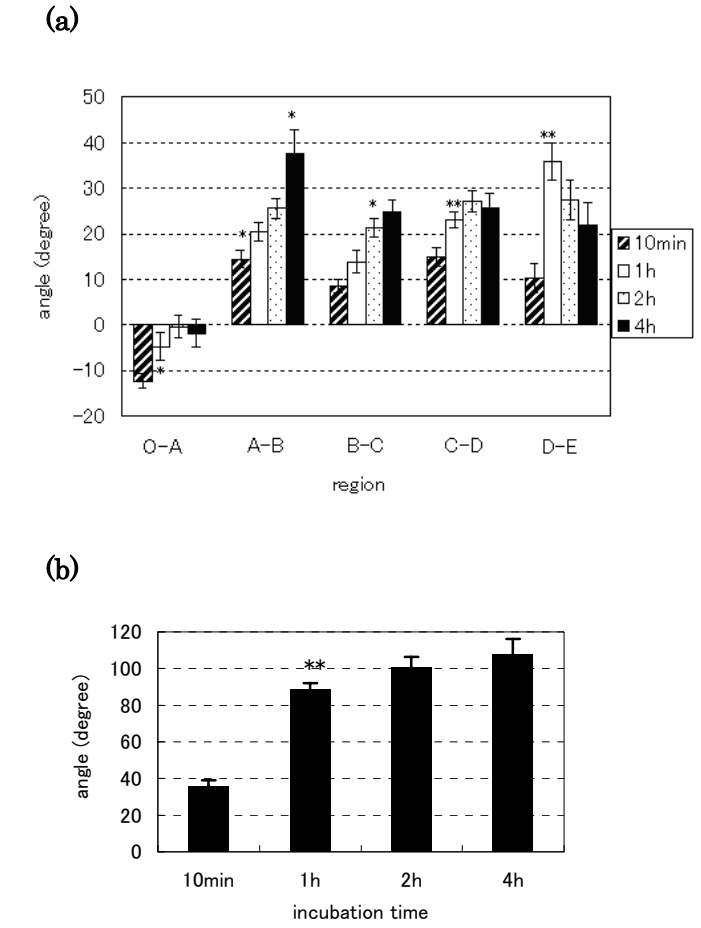

Fig. 2-3. Analysis for flagellar bending determining (a) the average bend angle in each flagellar region, and (b) the sum of the average bend angles for each region. Photographs were taken at 250 frames per 3 seconds. The analysis used 8 successive frames. To measure the regional bend angles in the flagellum, the image of the flagellum was divided as described in the legend for Figure 2-1. The regions between O and A, A and B, B and C, C and D, and D and E were termed O-A, A-B, B-C, C-D, and D-E, respectively. These parameters are described in the *Materials and Methods*. The experiments were repeated three times. The data were pooled and are expressed as the mean ± S.E.M. (n = 21). Asterisks indicate significant differences from the value at the previous time point (Student's *t*-test; **: $P < 0.01$ and *: $P < 0.05$).

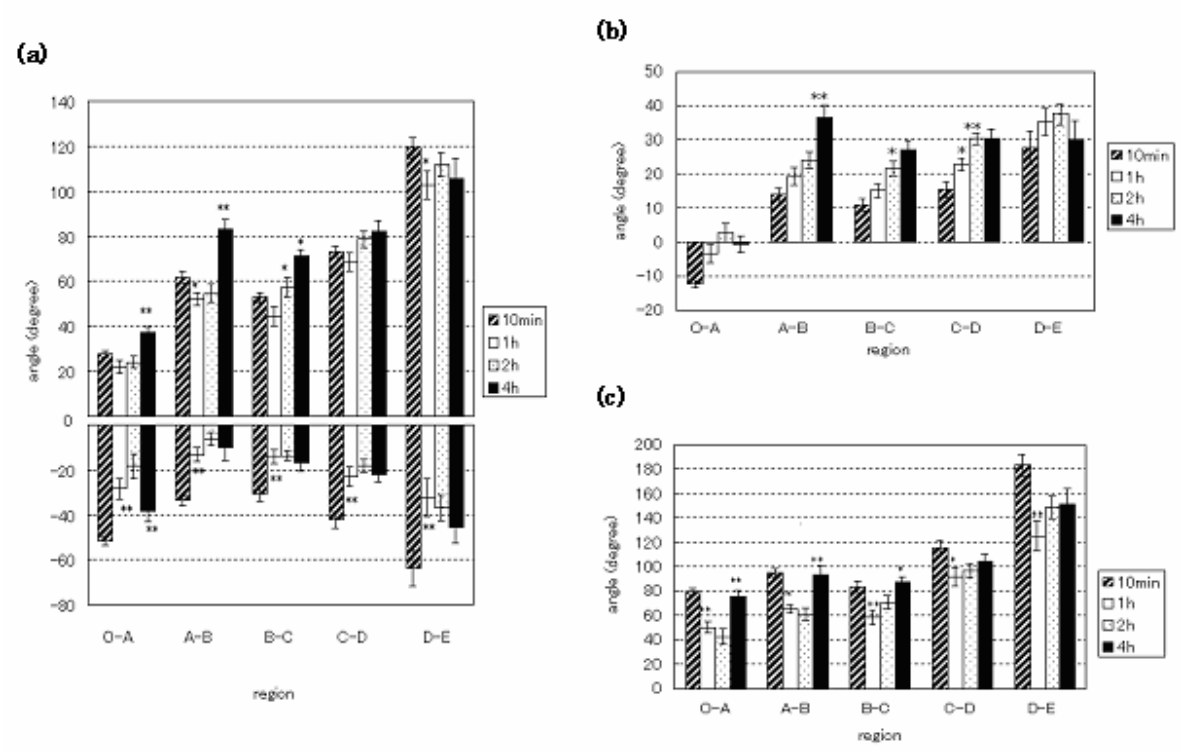

Fig. 2-4. Analysis for flagellar bending based on the maximum and minimum bend angles in each flagellar region. Photographs were taken at 250 frames per 3 seconds. The analysis used 8 successive frames. (a) The maximum and minimum regional bend angles. (b) The average of the maximum and minimum. (c) The difference between the maximum and minimum. The regions were defined as described in the legends for Figures 2-1 and 2-3. The parameters are described in the *Materials and Methods*. The experiments were repeated three times. The data were pooled and are expressed as the mean ± S.E.M. (n = 21). Asterisks indicate significant differences from the value at the previous time point (Student's *t*-test; **: $P < 0.01$ and *: $P < 0.05$).

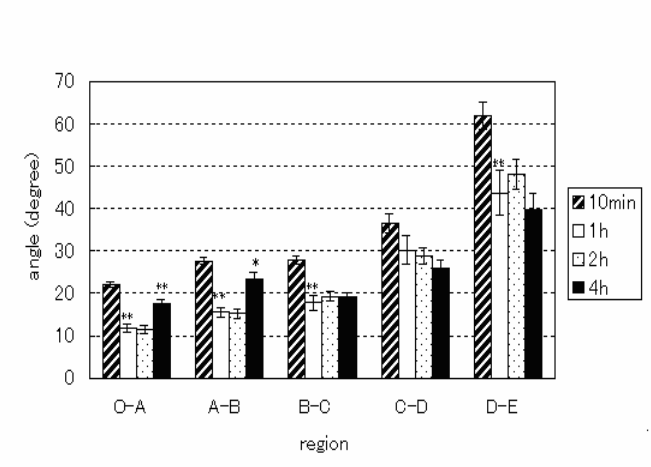

Fig. 2-5. Analysis for the changes in the bend angles between two successive frames in each region. Photographs were taken at 250 frames per 3 seconds. The analysis used 8 successive frames. The regions were defined as described in the legends for Figures 2-1 and 2-3. The parameters are described in the *Materials and Methods*. The experiments were repeated three times and similar results were obtained. The data were pooled and are expressed as the mean ± S.E.M. (n = 21). Asterisks indicate significant differences from the value at the previous time point (Student's *t*-test; **: $P < 0.01$ and *: $P < 0.05$).

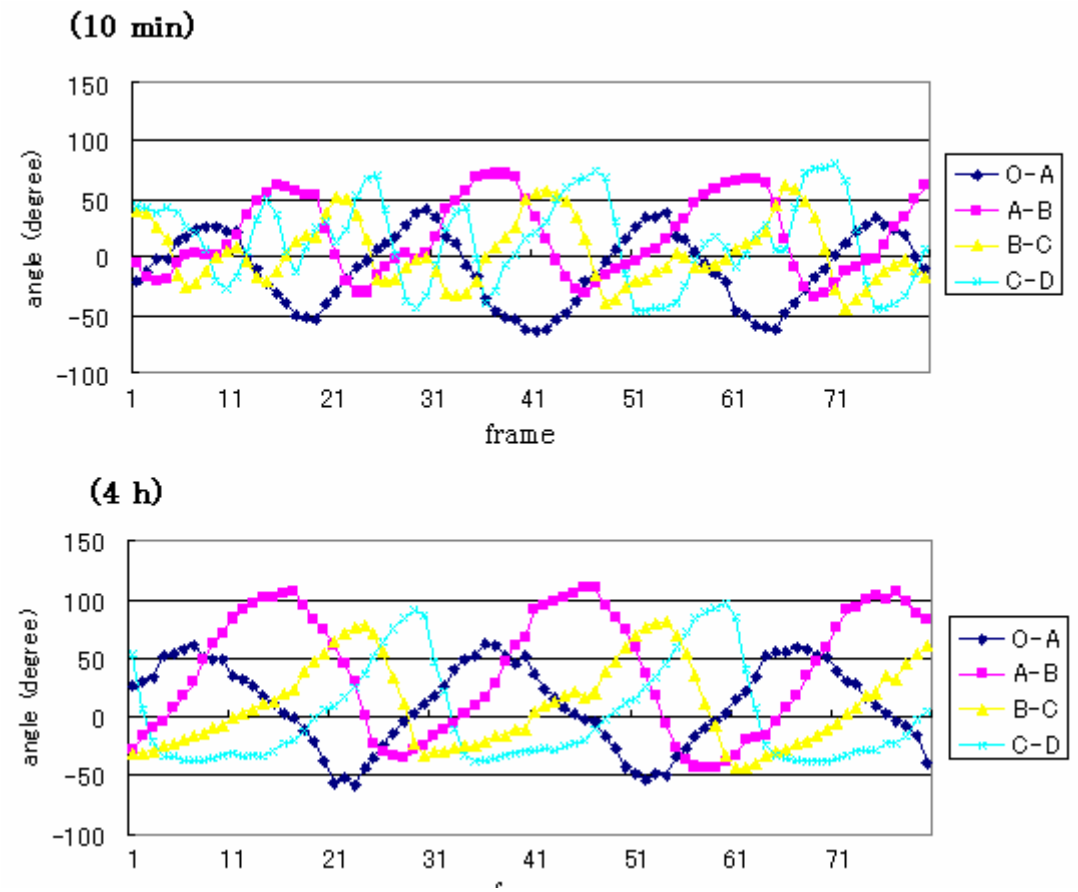

Fig. 2-6. Propagation of the wave on the flagellum. The spermatozoa were incubated for 10 min and 4 h. Photographs were taken at 250 frames per second and the time length between two adjacent frames was 1/250 s. The regions were defined as described in the legends for Figures 2-1 and 2-3. The parameters are described in the *Materials and Methods*. Three spermatozoa were analyzed in each experiment and similar results were obtained.

Fig. 2-7. Propagation of wave in each region of the flagellum. The spermatozoa were incubated for 10 min and 4 h. Photographs were taken at 250 frames per second and the time length between two adjacent frames was 1/250 s. The regions were defined as described in the legends for Figures 2-1 and 2-3. The parameters are described in the *Materials and Methods*. Three spermatozoa were analyzed in each experiment and similar results were obtained.

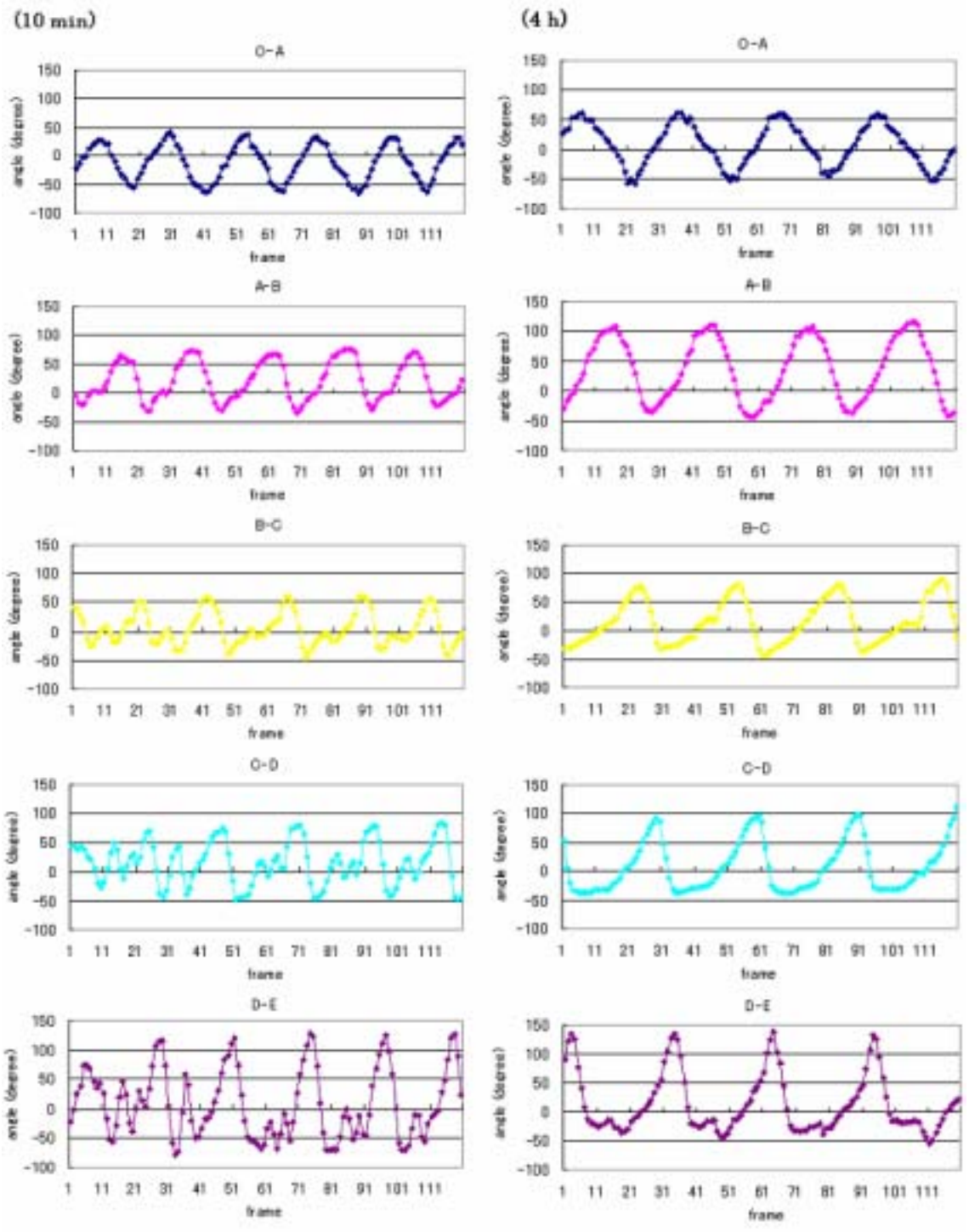
(10 min)
(4 h)
O-A
A-B
B-C
C-D
D-E
angle (degree)
frame
150
100
50
0
-50
-100
1 11 21 31 41 51 61 71 81 91 101 111

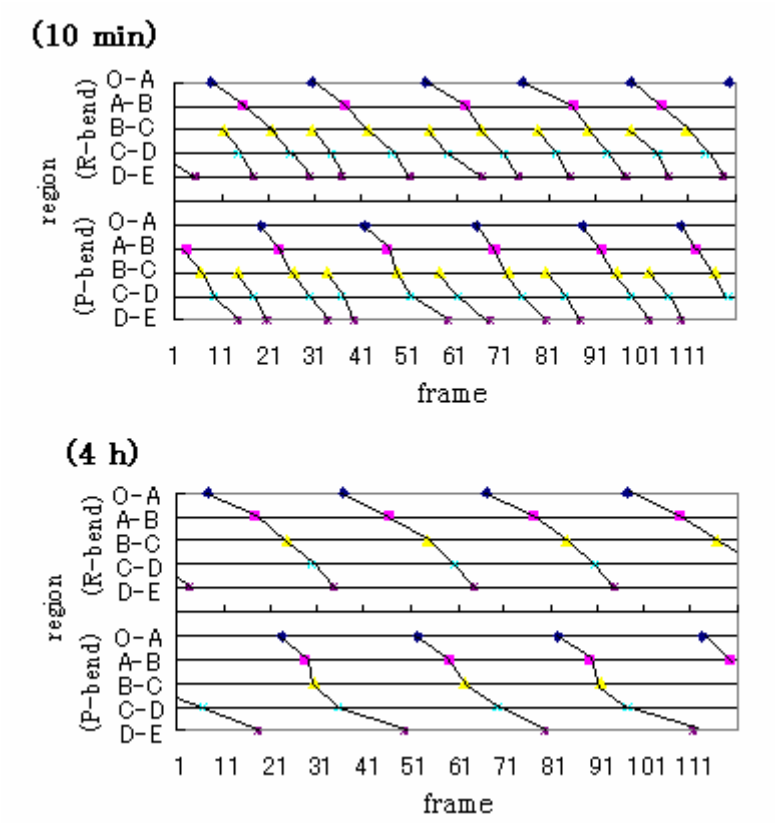

Fig. 2-8. Typical patterns of time point transmission of the maximum (R-bend maximum) and minimum (P-bend maximum) value. The spermatozoa were incubated for 10 min and 4 h. Photographs were taken at 250 frames per second and the time length between two adjacent frames was 1/250 s. The regions were defined as described in the legends for Figures 2-1 and 2-3. The parameters are described in the *Materials and Methods*. Three spermatozoa were analyzed in each experiment and similar results were obtained.

Fig. 2-9. Trajectories of whole flagellum in freely swimming spermatozoa. The spermatozoa were incubated for 10 min and 4 h. Photographs were taken at 250 frames per second. The trajectories of whole flagellum are indicated by black lines. The trajectory of position in A, B, C, and D on the flagellum, which were defined as described in the legend for Figure 2-1, is indicated by red line. Three spermatozoa were analyzed in each experiment and similar results were obtained.

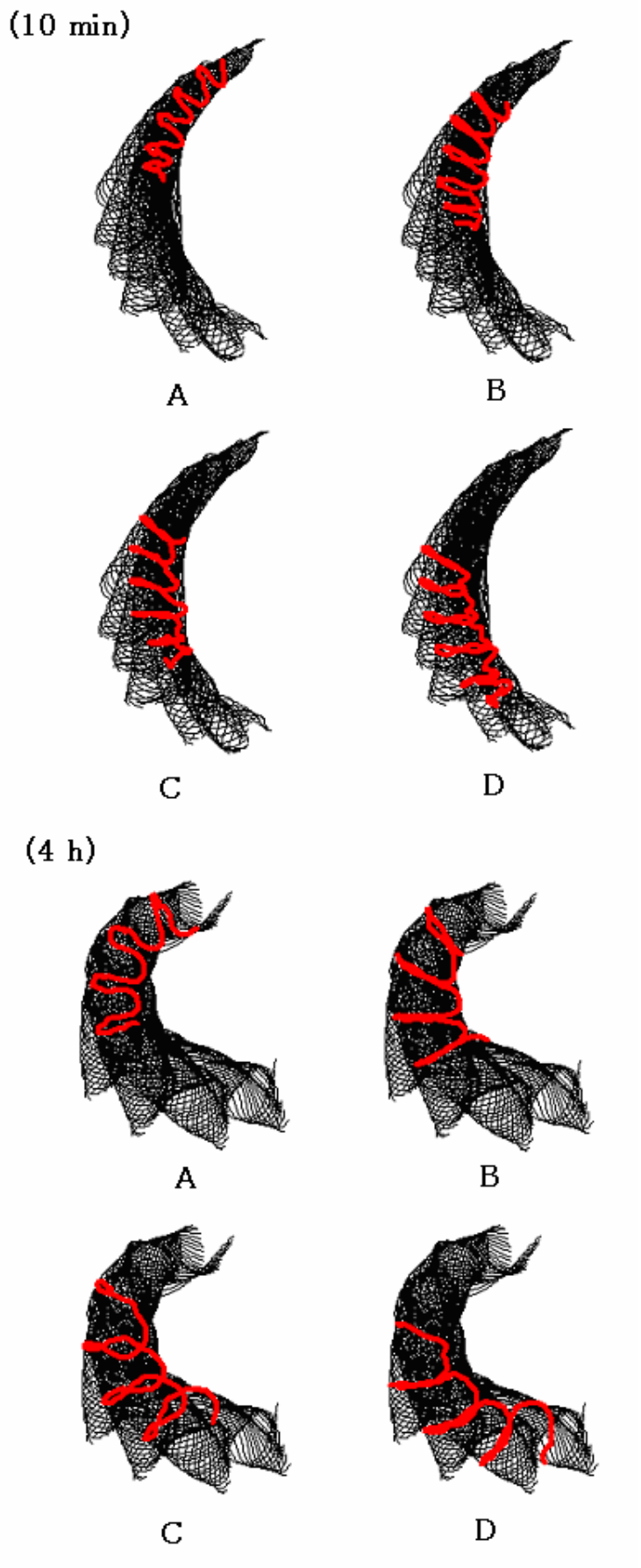
(10 min)
A
B
C
D
(4 h)
A
B
C
D

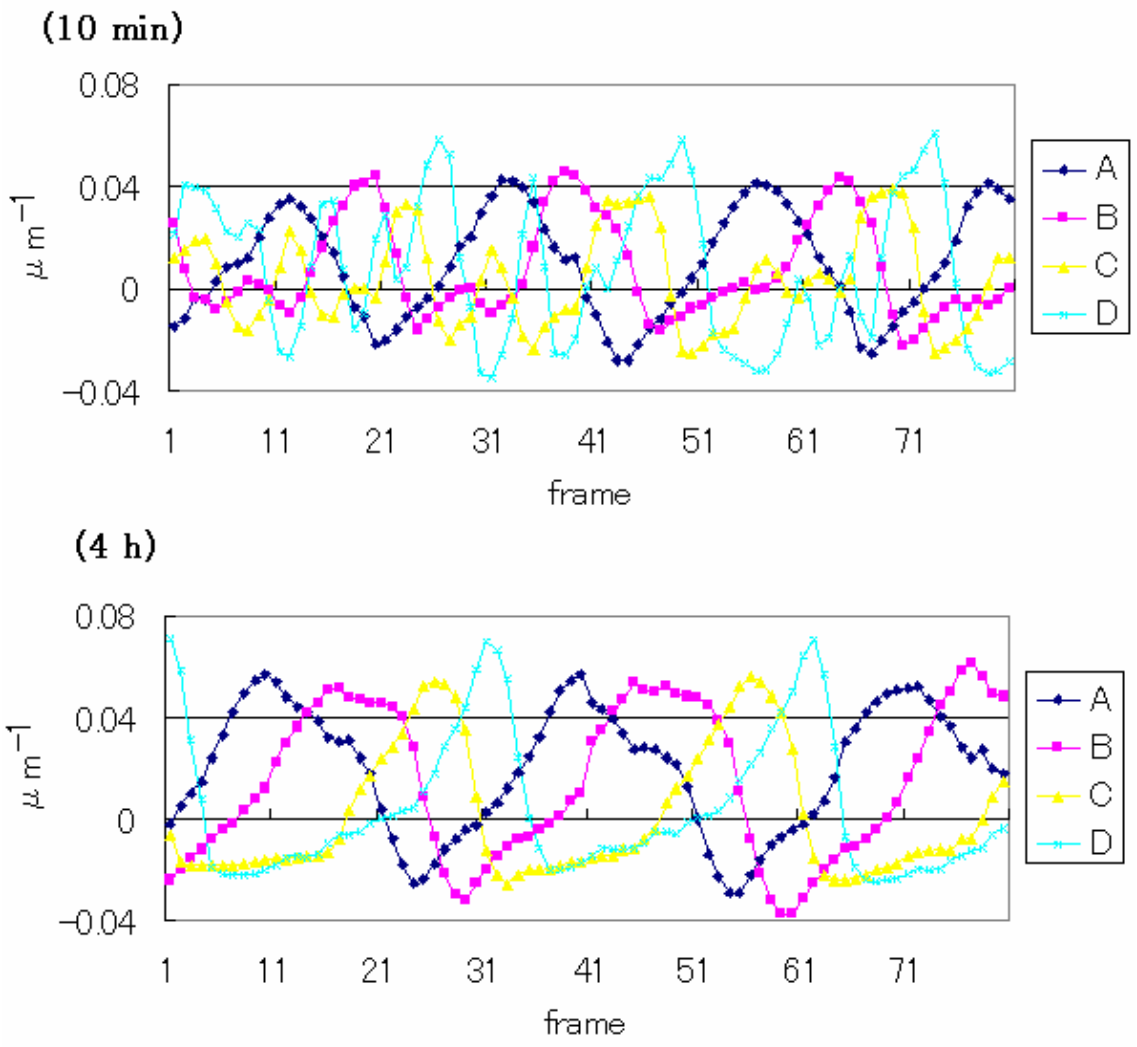

Fig. 2-10. Typical patterns of the curvature following the time course in each position of the flagellum. The spermatozoa were incubated for 10 min and 4 h. Photographs were taken at 250 frames per second and the time length between two adjacent frames was 1/250 s. The positions were defined as described in the legends for Figure 2-1. The parameters are described in the *Materials and Methods*. Three spermatozoa were analyzed in each experiment and similar results were obtained.

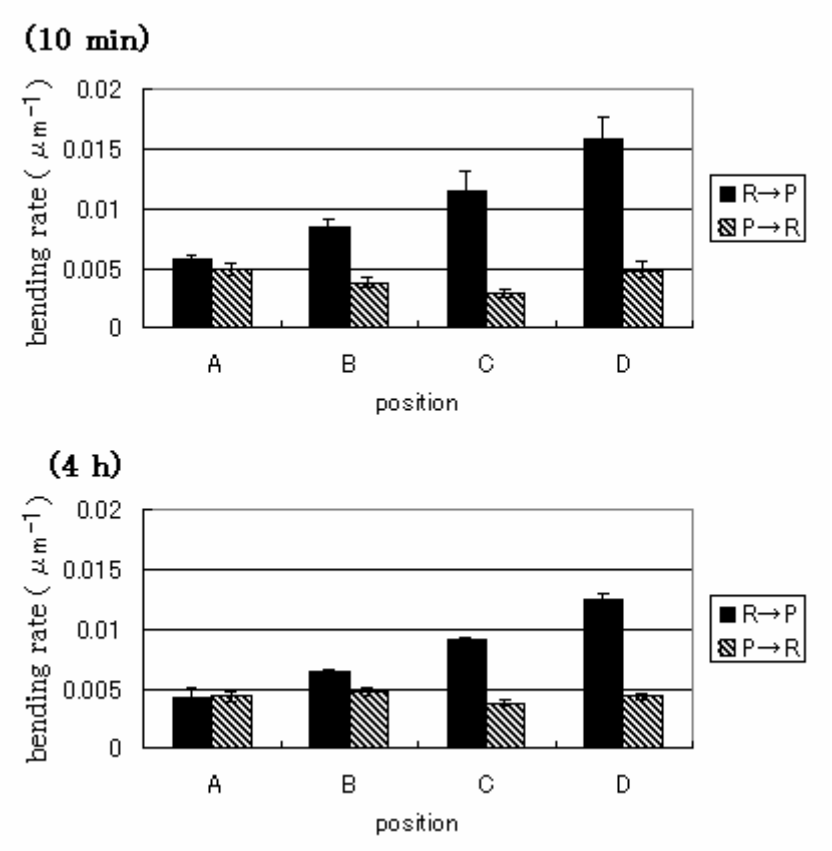

Fig. 2-11. The bending rate at each position on the flagellum. The spermatozoa incubated for 10 min and 4 h. Photographs were taken at 250 frames per second. Using more than 3 of the cycles of flagellar bending in 120 successive frames, the analysis was performed. The positions were defined as described in the captions to Figure 2-1. The parameters are described in the *Materials and Methods*. Three spermatozoa were analyzed in each experiment and the data are expressed as the mean ± S.E.M. (n = 3).

Fig. 2-12. Analysis for the curvature and propulsive force. The spermatozoa were incubated for 10 min and 4 h. Photographs were taken at 250 frames per second and the time length between two adjacent frames was 1/250 s. The changes in curvature and propulsive force were examined at the positions of B, C, and D on the flagellum in the spermatozoa. The propulsive force in positive value to the direction of movement is indicated by red dots and that in negative value by blue dots. Three spermatozoa were analyzed in each experiment and similar results were obtained.

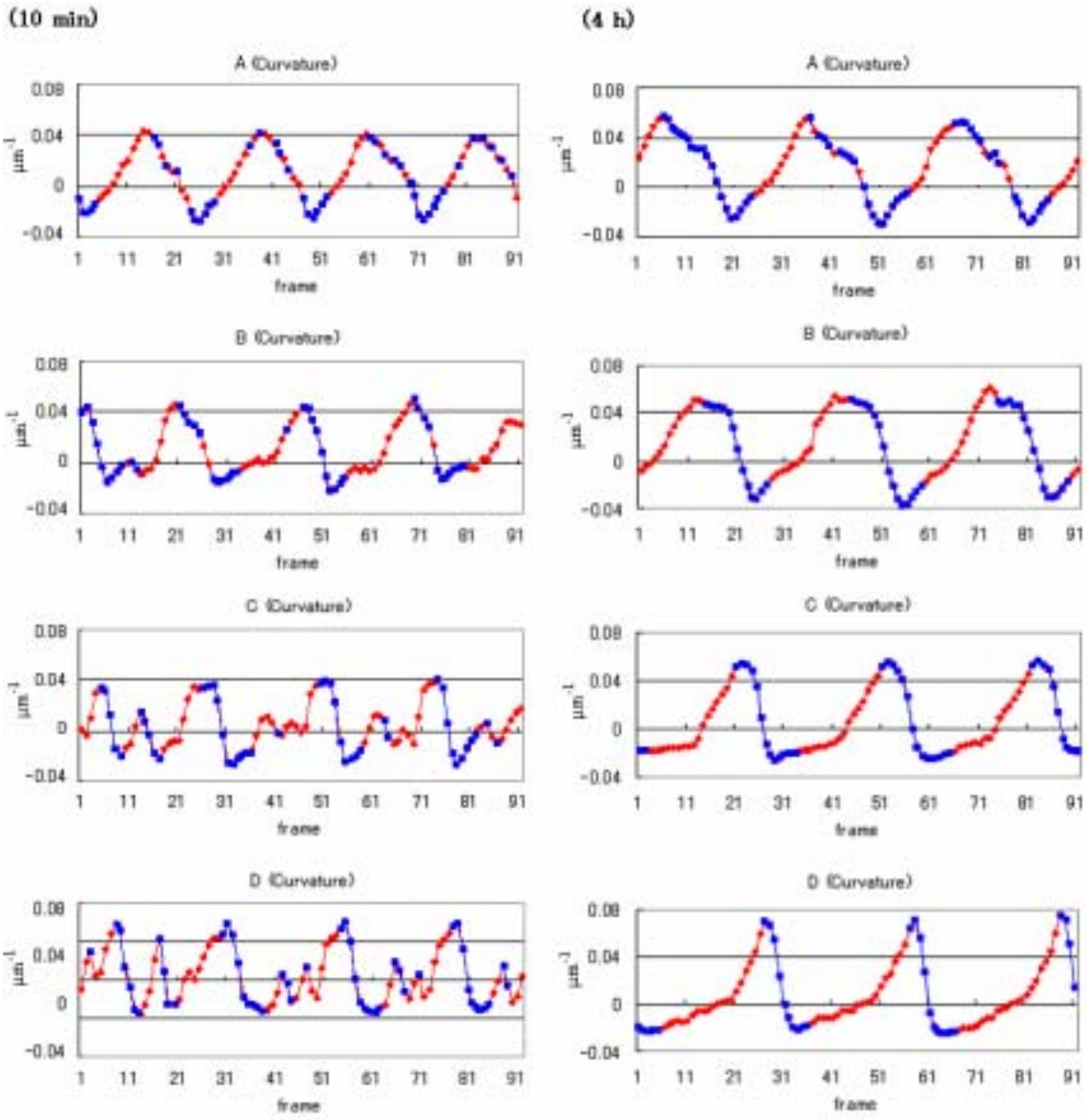
(10 min)
(4 h)
A (Curvature)
B (Curvature)
C (Curvature)
D (Curvature)
μm-1
frame
0.08
0.04
0
-0.04
1
11
21
31
41
51
61
71
81
91

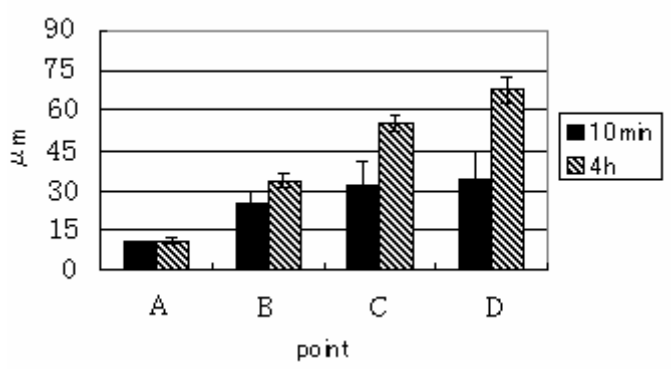

Fig. 2-13. Amplitude of the bending at each position on the flagellum in hamster spermatozoa. The spermatozoa were incubated for 10 min and 4 h. Photographs were taken at 250 frames per second and the time length between two adjacent frames was 1/250 s. The amplitude was measured by superimposing the axes of the heads. The analysis used 120 successive frames. The positions are defined as described in the legend for Figure 2-1. The experiments were performed three spermatozoa. The data are expressed as the mean ± S.E.M. (n = 3).

Chapter 3

Regulation of microtubule sliding and flagellar bending in demembranated hamster spermatozoa

Abstract

To understand the mechanism regulating the motility of spermatozoa, it would be important to investigate the conversion of the microtubule sliding into flagellar bending. In this chapter, I examined the microtubule sliding and flagellar bending distinctly by using the demembranated spermatozoa model. To examine the microtubule sliding, I developed a novel method using a high concentration of reducing agent by which microtubules were efficiently extruded. Using these methods, I examined the roles of cAMP, Ca^{2+}, and their target kinases in the regulation of flagellar bending and microtubule sliding. At a low cAMP concentration, microtubule extrusion but not flagellar bending was observed, suggesting that cAMP is necessary for the conversion of microtubule sliding into flagellar bending but not for microtubule sliding itself. The target of cAMP regulating the flagellar bending was not cAMP dependent protein kinase (PKA), since flagellar bending was still observed in the spermatozoa treated with PKA specific inhibitor. Alternatively, Epac/Rap pathway, which is one of the other targets of cAMP may be involved, since Epac2 and Rap2 were detected in hamster spermatozoa by immunoblotting. In terms of Ca^{2+}, microtubule extrusion but not flagellar bending was observed at 10^{-4}-10^{-3} M, suggesting that high concentration of Ca^{2+} have a detrimental effect on the conversion of microtubule sliding into flagellar bending. The target of Ca^{2+} was neither Ca^{2+} dependent protein kinase (PKC) nor calmodulin, since their inhibitors did not attenuated the inhibition by Ca^{2+}. Finally, PKC seemed to be involved in the regulation of microtubule sliding independently of Ca^{2+}. An inhibitor of PKC completely inhibited the microtubule extrusion in a Ca^{2+}-free condition. Thus, analyzing separately microtubule sliding and flagellar bending is useful to elucidate the molecular mechanism regulating the motility of spermatozoa.

Introduction

The propulsive force of spermatozoa for the progressive swimming is generated by flagellar bending, which is regulated *via* the activation of the flagellar axoneme. In the chapter 2, I investigated the mechanism by which flagellar bending generates the propulsive force. In this chapter, I investigate the mechanism by which flagellar bending is generated. The generation of flagellar bending would consist of two processes, in which individual doublet microtubules slide *via* the activation of dynein arm and then the sliding of microtubules is converted into flagellar bending. Therefore, to elucidate the mechanism by which flagellar bending is generated, it is important to examine both the microtubule sliding and its conversion into flagellar bending.

The demembranated spermatozoa model is useful for the investigation of the component required for activation of the flagellar axoneme. In the spermatozoa that are demembranated with the nonionic detergent Triton X-100, flagellar movement that is comparable to that of intact spermatozoa can be reproduced in the presence of Mg^{2+}-ATP (Lindemann and Gibbons, 1975). Individual microtubule sliding produced by dynein ATPase activity has been demonstrated in the demembranated spermatozoa model after partial digestion of the axoneme proteins with proteases. Treatment with an appropriate concentration of trypsin (Si and Okuno 1993, 1995) or elastase (Ishijima *et al*., 2002; Nakano *et al*., 2003) in the presence of Mg^{2+}-ATP induces microtubule extrusion. Electron microscopic analysis has revealed that protease treatment digests the axonemal structural proteins, thereby disrupting both the nexin links and the radial spokes. However, it seems likely that proteases also degrade other important regulatory components that are involved in flagellar bending. Thus, microtubule extrusion induced by protease digestion does not appear to be the best model for the investigation of the regulatory mechanisms of microtubule sliding.

The molecular mechanisms by which spermatozoa regulates their motility remain unclear. There are some reports suggesting that protein phosphorylation is

involved in the regulation of spermatozoa motility. Protein phosphorylation could be an important post-translational event regulating spermatozoa motility, which is mediated by cAMP and Ca^{2+}. The activation of cAMP dependent protein kinase and stimulation of protein phosphorylation was shown to be involved in the initiation and maintenance of motility (Brandt and Hoskins, 1980; Noland *et al*., 1987; Bookbinder *et al*., 1991). The initiation of motility is regulated by the tyrosine phosphorylation of a 15 kDa protein, which is stimulated by cAMP in the rainbow trout spermatozoa (Morisawa and Hayashi, 1986; Hayashi *et al*., 1987). A-kinase anchoring proteins (AKAPs) are scaffold proteins for cAMP dependent kinase and the disruption of the Akap4 causes the defects in the spermatozoa motility (Miki *et al*., 2002). Ca^{2+} seems to regulate spermatozoa motility *via* protein phosphorylation. In fowl spermatozoa, decrease in intracellular free Ca^{2+} concentration reduced the spermatozoa motility and changed the profile of protein phosphorylation (Ashizawa *et al*., 1992; Ashizawa *et al*., 1994). Ca^{2+} inhibited the spermatozoa motility and reduced the overall level of protein phosphorylation (Tash and Means, 1982). Calmodulin and calmodulin-dependent protein kinase II, which is a target of Ca^{2+}, induce the flagellar motility in *Chlamydomonas* (Smith, 2002) and *ascidian* (Nomura *et al*., 2004). Although there are thus many reports demonstrating that cAMP, Ca^{2+} and their target kinases are involved in flagellar motility, little is known about their effects on microtubule sliding in the demembranated spermatozoa.

In this chapter, to clarify the mechanism by which flagellar bending is generated, I examined the microtubule sliding and flagellar bending by using the demembranated spermatozoa model. In the analysis for microtubule sliding, I developed a novel method that was likely to produce minimal digestion of axonemal proteins. Using these methods, I examined the role of cAMP, Ca^{2+}, and their target kinases in the regulation of flagellar bending and microtubule sliding.

Materials and Methods

Spermatozoa preparation

Sexually matured hamsters were killed by chloroform inhalation. The cauda epididymis was promptly removed. After removing any blood from the epididymal surface with physiological salt solution, the distal tubules were punctured with an 18-gauge needle in five to ten places, and a mass of spermatozoa squeezed out with forceps into a plastic Petri dish (35 mm x 10 mm). The hamster semen was covered with mineral oil that had been pre-warmed to 37 ºC, in order to prevent evaporation before use.

Procedure for reactivation and the induction of microtubule extrusion in the demembranated spermatozoa

Demembranation and reactivation of spermatozoa was performed using a modification of the method developed by Ishijima and Witman (1991). A 1 µl of aliquot of semen was suspended in 100 µl of demembranation medium that contained 1 mM EDTA, 50 mM N-2-hydroxyethyl-piperazine-N-2-ethane sulphonic acid (HEPES, pH 7.9), and 0.2 % (w/v) Triton X-100. The suspension was incubated for 30 s with gentle stirring at 37 ºC to dissolve the plasma membrane and mitochondrial sheath. The demembranated spermatozoa thus obtained were reactivated by transferring 10 µl of the suspension of demembranated spermatozoa to 100 µl of the reactivation medium that contained 1 mM EDTA, 1 mM ATP, 5 mM $MgCl_2$, 50 µM cAMP, and 50 mM HEPES (pH 7.9). In the induction of microtubule extrusion, a protease inhibitor cocktail that contained 1 µg/ml aprotinin, 2 µg/ml leupeptin, 1 µg/ml pepstatin, and 100 µl/ml phenylmethyl sulfonyl fluoride was added to the demembranation and reactivation media. To induce microtubule extrusion 33 mM of dithiothreitol (DTT) was added to the reactivation medium. The free Ca^{2+} concentration was calculated using the computer program CALCON (Tash and Means, 1987) which is based on the algorism published

by Goldstein (1974). Spermatozoa were treated with phosphodiesterase (Sigma-Aldrich Japan K.K.Tokyo, Japan), cAMP-dependent protein kinase (PKA) inhibitor, N-[2-(p-Bromocinnamylamino)ethyl]-5-isoquinolinesulfonamide (H89, SEIKAGAKU Co., Tokyo, Japan), Protein kinase C (PKC) inhibitory peptide (V5691, Promega Co., WI, USA), and calmodulin antagonist, N-(4-aminobutyl)-5-chloro-2-naphthalene sulfonamide (W-13, SEIKAGAKU Co.).

Microscopic observation of spermatozoa

After the reactivated spermatozoa were incubated at 37 ºC for more than 10 min, 10 µl of each spermatozoa suspension were placed on a glass slide pre-warmed to 37 ºC and covered with an 18 x 24 mm coverslip. As soon as the sample was prepared, photographs were taken at 60 frames per second and an exposure time of 1/1000 s, with a FASTCAM-Net high-speed camera (PHOTRON, Tokyo, Japan) on a phase-contrast microscope. The images obtained were recorded using Movie Ruler (PHOTRON). Spermatozoa were selected for the analysis at random.

Determination of the reducing power of DTT and 2-ME

To investigate the reducing power of DTT and 2-ME, various concentrations of each agent were used to reduce IgG, and the resulting protein conformations were analyzed by non-reducing SDS-PAGE. Whole goat IgG (Jackson ImmunoResearch Laboratories Inc, West Grove, PA, USA) was added in 100-µl aliquots to microcentrifuge tubes that contained 500 µl of reactivation medium plus various concentrations of DTT or 2-ME. After incubation for 10 min at 37 ºC, the proteins were precipitated with an equal volume of 10 % (w/v) trichloroacetic acid. Each sample was centrifuged at 10,000 xg for 10 min at 4 ºC, and the supernatant was discarded. The pellet was washed with 5 % (w/v) trichloroacetic acid and again centrifuged at 10,000 xg for 10 min at 4 ºC. After discarding the supernatant, the pellet was dissolved in 25 µl of 0.1 N NaOH and the pH was adjusted by the addition of 15 µl of 0.1N HCl. Then, 40

μl of x2 SDS sample buffer (Laemmli, 1970) without 2- ME were added to each sample and the mixtures were boiled for 1 min. The samples were subjected to electrophoresis on 7.5 % SDS-PAGE gels, along with pre-stained SDS-PAGE molecular weight standards (Bio-Rad Laboratories, Inc., Hercules, CA, USA). The gels were fixed and stained with Coomassie brilliant blue R-250. After staining, the gels were dried for 2 h at 80 ºC.

PKA activity

A 1 μl of aliquot of semen was suspended in 200 μl of demembranation medium consisting of 1 mM EDTA, 50 mM N-2-hydroxyethyl-piperazine-N-2-ethane sulphonic acid (HEPES, pH 7.9), 0.2 % (w/v) Triton X-100, and a protease inhibitor cocktail that contained 1 μg/ml aprotinin, 2 μg/ml leupeptin, 1 μg/ml pepstatin, and 100 μl/ml phenylmethyl sulfonyl fluoride. The suspension was incubated for 30 s with gentle stirring at 37 ºC to dissolve the plasma membrane and mitochondrial sheath. Then, 10 μl of the suspension of extracted spermatozoa were transferred to 90 μl of the kinase reaction buffer consisting of 100 μM kemptide (Kemp *et al*., 1977), 1 mM EDTA, 5 mM $MgCl_2$, and 50 mM HEPES (pH 7.9), the protease inhibitor cocktail, and various concentrations of c AMP. Assays were initiated by the addition of 2 μl of 16.5 μM [γ-^{32}P] ATP containing 133 KBq/ml (Amersham Pharmacia Biotech UK Ltd., Buckinghanshire). After incubation for 10 min at 37 ºC, the suspensions were centrifuged at 12,000 xg for 1 min. Twenty μl of the supernatant was then spotted on P81 paper square. After left at room temperature for 30 s, the papers were washed with 0.75 % phosphoric acid three times. Then the papers were washed with acetone and air dried. They were analyzed by Cerenkov counting. The kinase activity is expressed as cpm of ^{32}P incorporated into kemptide.

Immunoblotting

Each 200 μl of the spermatozoa suspension was centrifuged at 3,000 xg for 5

min and the pellets were added with 80 μl of extraction buffer consisting of 50 mM Tris-HCl, 150 mM NaCl, 1 % Nonidet P-40, 0.5 mM EDTA, 100 μM sodium orthovanadate, 0.1 % SDS, 1 mM DTT, 1 μg/ml aprotinin, 2 μg/ml leupeptin, 1 μg/ml pepstatin, and 100 μg/ml phenylmethylsulfonyl fluoride (pH 8.0), and freezed at –20 ºC. After thawed, the suspensions were denatured for SDS-PAGE as follows. The suspensions were added with 80 μl of extraction buffer, 50 μl of x4 SDS sample buffer and 96 mg of urea, and then boiled for 1 min. These samples were subjected to electrophoresis on 10 % SDS-PAGE gels. The proteins were electroblotted to a polyvinylidene difluoride membrane (Millipore Corp., Bedford, MA). Non-specific binding on the membrane was blocked with 5 % BSA in Tris-buffered saline (TTBS; 150 mM NaCl, 20 mM Tris-HCl, and 0.1 % Tween 20, pH 7.6) for 1 h at room temperature. The blot was kept overnight at 4 ºC with polyclonal anti-Epac2 (sc-9384, Santa Cruz biotechnology) and anti-Rap2 (R23020, Transduction Laboratories) antibody (2 μg/ml in TTBS). To confirm the specificity, the primary anti-Epac2 antibody was neutralized with 10 μg/ml of antigen peptide (sc-9384s, Santa Cruz biotechnology). The blot was then washed with TTBS three times for 10 min each and kept 1 h at room temperature with horseradish peroxidase-conjugated sheep anti-mouse IgG at 1:1000 dilution. After 1 h at room temperature, the membrane was washed with TTBS three times, 20 min each, and the peroxidase activity was detected by using LAS-1000plus (Fuji Photo Film Co. Ltd., Tokyo) and the images obtained were recorded using Image Gauge (Fuji Photo Film Co. Ltd., Tokyo).

Results

Establishment of the procedure for efficient induction of microtubule extrusion by reducing agents

In order to minimize protein digestion by endogenous proteases, the protease inhibitor cocktail was added to the demembranation and reactivation media. In the presence of protease inhibitors, microtubule extrusion occurred in hamster spermatozoa upon the addition of reducing agents to the reactivation medium. The extrusion was observed in some spermatozoa at concentrations of 3.3 mM in DTT and 33 mM in 2-ME and in most spermatozoa at greater than 10 mM in DTT and 100 mM in 2-ME (Fig. 3-1a and 3-2).

The concentrations of DTT and 2-ME required to induce the extrusion of microtubules thus differed by 10-fold (Fig. 3-1a). This difference appears to be due to the different reducing potencies of two agents. To confirm this, I examined the reducing powers of DTT and 2-ME using IgG as the substrate. As shown in Figure 3-1b, the dense 150 kDa electrophoretic band, which corresponds to the intact form of IgG, was eliminated by treatment with concentrations greater than 3.3 mM DTT or 33 mM 2-ME. This result confirms that the disulfide bonds in IgG are reduced by treatment with DTT or 2-ME, and that the effective concentration of 2-ME is 10-fold higher than that of DTT.

Characteristics of microtubule extrusion induced by reducing agents

The process of microtubule extrusion was closely observed by phase-contrast microscopy. In the presence of 33 mM DTT, microtubules were always extruded from midpiece region, especially around the head-midpiece junction and midpiece-principal piece junctions (Fig. 3-2).

Extrusion appeared to be on the same side as, and/or the opposite side of the curve of, the spermatozoal heads. Thus, extrusion occurred in the same plane as that in

which flagellar bending occurs in intact spermatozoa (Aoki *et al*., 1994). Extrusion always began on only one side and was followed by extrusion on the other side; extrusion never occurred simultaneously on both side (Fig. 3-3a). In some spermatozoa, intrusion, *i.e.* return to the normal position within the flagellar axoneme, of some extruded microtubules was observed when microtubules were extruded on the opposite side (Fig. 3-3b).

The effect of cAMP on microtubule extrusion and flagellar bending

A number of literatures demonstrated that cAMP is necessary for flagellar bending (Lindemann, 1978; Morisawa and Okuno, 1982; Ishiguro *et al*., 1982; Opresko and Brokaw, 1983; Tash *et al*., 1984; Tash *et al*., 1986), although its necessity for the microtubule sliding has not been examined. Consistent with the results reported in those literatures, flagellar bending was not observed in the demembranated spermatozoa without cAMP (Fig. 3-4). When 0.1 μM cAMP was added into the reactivation medium, flagellar bending was observed in 14 % of spermatozoa. At the concentration of greater than 1 μM, it was observed in 60 % of spermatozoa. However, microtubule extrusion occurred in the reactivation medium without cAMP. Cyclic AMP did not show any effect on the extrusion. More than 80 % of spermatozoa always extruded microtubules at any concentrations of cAMP in the reactivation medium, even in the cAMP-free medium containing cAMP phosphodiesterase which degrades cAMP (Fig. 3-4). These results indicate that cAMP is involved in flagellar bending, but not in microtubule sliding. Cyclic AMP has an essential role for the conversion of microtubule sliding into flagellar bending.

Although it is known that the activation of PKA is cAMP dependent and I confirmed that PKA activity increased with a cAMP concentration in the suspension of demembranated spermatozoa (Fig. 3-5a), flagellar bending was still observed when 10 μM of H89, PKA specific inhibitor, was added into the demembranation and reactivation media (Fig. 3-5b). By the treatment with 50 μM of cAMP plus 10 μM of

H89, PKA activity was completely inhibited (Fig. 3-5c), but the percentage of the spermatozoa which showed flagellar bending was not changed (Fig. 3-5b). Thus, the target of cAMP that was involved in flagellar bending was not PKA activity in the demembranated hamster spermatozoa.

To investigate the target of cAMP other than PKA, I examined Epac/Rap pathway, since recent reports demonstrated that this pathway is stimulated by cAMP in the somatic cells (Rangarajan *et al*., 2003; Enserink *et al*., 2004). In the immunoblotting analysis for Epac and Rap, specific dense bands at 110 kDa for Epac2 and 22 kDa for Rap2 were detected in the hamster spermatozoa. The 110 kDa band for Epac2 was specific, since it disappeared by neutralization with antigen peptide against anti-Epac2 antibody (Fig. 3-6). The specificity for the antibody against Rap2 was not examined because the antigen was not available. Epac1 and Rap1 were not detected (data not shown). These results suggest that Epac2/Rap2 pathway is involved in the conversion of microtubule sliding into flagellar bending.

The effects of Ca^{2+} on microtubule extrusion and flagellar bending

The effects of Ca^{2+} on the microtubule sliding and flagellar bending were examined at the various concentrations of Ca^{2+} in the reactivation medium. In the demembranated spermatozoa, microtubule extrusion and flagellar bending were observed in the Ca^{2+}-free medium containing 10 mM of EGTA which completely chelate Ca^{2+}. The percentage of spermatozoa showing flagellar bending decreased at 10^{-5} M of Ca^{2+} and only a small part of spermatozoa showed flagellar bending at 10^{-4} M and higher concentration, while microtubule extrusion was not inhibited even at 10^{-3} M: it was inhibited at 10^{-2} M (Fig. 3-7). Thus, Ca^{2+} seems to be involved in the regulations of microtubule sliding and flagellar bending by different mechanisms.

The mechanism for the inhibitory effects of a high concentration of Ca^{2+} on the microtubule sliding and flagellar bending were examined by using the inhibitor of protein kinase C and calmodulin. The inhibition of microtubule sliding and flagelar

bending were still observed in the demembranated spermatozoa treated with 50 μM of PKC inhibitor, which is a peptide with the sequence of pseudosubstrate region in PKC, and 200 μM of W-13, calmodulin specific inhibitor. Thus, PKC and calmodulin do not seem to be involved in Ca^{2+} dependent mechanism regulating the microtubule sliding and flagellar bending.

Suprisingly, at low Ca^{2+} concentration, even in the Ca^{2+}-free medium containing 10 mM of EGTA, microtubule extrusion and flagellar bending were inhibited by the treatment with PKC inhibitor in the demembranated hamster spermatozoa. The spermatozoa showed neither the microtubule extrusion nor flagellar bending when they were treated with the concentration greater than 33 μM of PKC inhibitor (Fig. 3-8). At this concentration, the spermatozoa were completely motionless. Thus, PKC which is independent of Ca^{2+} seems to be involved in the regulations of basal microtubule sliding.

Discussion

There are many reports describing the various factors which are involved in the flagellar bending of spermatozoa (see review, Woolley, 2000; Ho and Suarez, 2001; Luconi and Baldi, 2003). However, few reports have described the factors which are involved in the regulation of microtubule sliding, although microtubule sliding is a basal process to generate the flagellar bending. In the present study, I developed the methods to separately investigate microtubule sliding and the conversion into flagellar bending. By treating the demembranated spermatozoa with and without DTT, the microtubule sliding and flagellar bending, respectively, could be separately investigated. Using these methods, I showed that cAMP and Ca^{2+} were involved in the mechanism by which microtubule sliding is converted into flagellar bending.

In the method which I established in this study, the microtubule extrusion was efficiently induced in the demembranated hamster spermatozoa following treatment with a reducing reagent alone. Based on previous studies, proteases such as trypsin (Summers and Gibbons, 1973; Brokaw and Simonick, 1977; Olson and Linck, 1977; Si and Okuno, 1993, 1995) and elastase (Brokaw 1980; Ishijima *et al*., 2002) were considered to be useful inducers of microtubule extrusion. However, in the current study, I have shown that treatment with a reducing agent is effective in inducing microtubule extrusion, and that trypsin has a rather detrimental effect on this process. Since the concentrations of the reducing agents required for the induction of microtubule extrusion corresponded to those sufficient to reduce the disulfide bonds of IgG (Fig. 3-1b), I speculate that microtubule extrusion is induced by the reduction of disulfide bonds in the proteins that connect the microtubules. A previous study demonstrated that the percentage of spermatozoa that extruded microtubule was much higher after treatment with DTT alone than after treatment with trypsin plus DTT (Kinukawa *et al*., 2004). In DTT treated spermatozoa, microtubule extrusion and intrusion, which were observed alternately (Fig. 3-3). However, in the trypsin-treated spermatozoa, the

intrusion of microtubules never occurred after the microtubules were extruded. These results suggest that proteases treatment digests one or more regulatory proteins involved in microtubule sliding, as well as proteins that connect the microtubules. Since the present method is likely to produce minimal digestion of axonemal proteins, it should find application in investigations of proteins that regulate motility, such as the microtubule-binding proteins.

The occurrence of intrusion as well as extrusion of microtubule (Fig. 3-2b) suggests the bidirectional force generation of dynein arms in the flagellum. Electron microscopic observation of trypsin-treated *Tetrahymena* cilia revealed that dynein arms generate force in only one direction, *i.e.* from the base to tip (Sale and Satir, 1977). However, my observations suggest that flagelalr microtubule slide in two directions, from base to tip and from tip to base, and that dynein arms generate forces in both directions. These differences in generated force direction may account for the different patterns of bending observed between cilia and flagella.

The mechanism by which microtubule sliding is converted into alternating flagellar bending to produce the propulsive force remains unclear. Nevertheless, the 'switch-point' hypothesis, originally advocated by Satir (Satir, 1985; Holwill and Satir 1994) offers an explanation for this phenomenon. This hypothesis proposes that the active bundles of the dynein arms switch, in an alternating fashion, from one side of the flagellum to the opposite side of the flagellum. The mechanistic framework of this hypothesis was explained in the Geometric Clutch hypothesis proposed by Lindemann (1994). When dynein-tubulin bridges form, they produce an adhesive force between adjacent doublets. The bridges pull adjacent doublets slightly closer together, and attachment of the bridges increases the chance for the neighboring dynein heads to also attach to each other. Conversely, detachment of the bridges increases the probability of further detachment of neighboring dynein heads by decreasing the total adhesive force that holds the doublets together. Thus, active dynein engagement on one side of the axoneme inhibits engagement on the opposite side, which results in an alternating

switching of the active dyneins. In support of this theory, the bundles of doublets 9-1-2 or those of doublets 5-6-7 are usually extruded, whereas both groups of the ATP-disintegrated macrocilia of the ctenophore *Beroe* are not extruded (Tamm and Tamm, 1984). Nakano *et al*. (2003) used electron microscopy to show that only one of the two opposed microtubule bundles (the 5-7 or 4-7 bundle, or the 9-2 or 9-3 bundle) was displaced in sea urchin spermatozoa that extruded microtubules after treatment with trypsin. These results suggest that only those microtubules that are located on one side of the flagellum are activated for sliding at any given moment, while those on the other side are inactive, thereby producing an alternating pattern. Furthermore, Lindemann *et al*. (1992) showed that microtubule bundle 9-2, which produces a bending force in the direction opposite to that of the curve of the head, was extruded in demembranated rat spermatozoa when the flagella were asymmetrical bent in the opposite direction of the curve. My results also support the 'switch-point' hypothesis: that microtubules could be extruded from the same side as that of curve of the spermatozoal head, as well as from the opposite side (Fig. 3-2). Furthermore, the extrusion always began on only one side, and was followed by extrusion on the other side, but never occurred simultaneously on both sides (Fig. 3-3), which lends support to the hypothesis by Lindemann (1994) that active dynein engagement on one side of the axoneme inhibits engagement on the opposite side.

For producing the flagellar bending to generate the propulsive force, the individual microtubule sliding is necessary to be converted into the coordinated sliding of microtubules. According to the "switch-point" hypothesis, the active bundles of the dynein arms switch, in an alternating fashion, from one side of the flagellum to the opposite side of the flagellum (Satir, 1985; Holwill and Satir 1994). The coordination of the alternating switch between active and inactive bundles would be necessary for the conversion the microtubule sliding into flagellar bending. The central C1 microtubule defined the location of active bundles of microtubule doublets (Wargo and Smith, 2003).Then, the system of central pair and the radial spokes play important roles in the

motility of 9+2 axomene (Witman *et al*., 1978; Sturgess and Chao, 1982; Neugebauer *et al*., 1990). Therefore, the interaction among the components of flagellum such as central apparatus, radial spokes, and dynein would be necessary for converting the individual microtubule sliding into flagellar bending which enables to generate the propulsive force. The results in this chapter suggested that cAMP and Ca^{2+} play important roles in the mechanism regulating the conversion of the microtubule sliding into flagellar bending but not for the microtubule sliding itself. In the reactivation medium without cAMP, the flagellar bending was inhibited but the microtubule extrusion was not in the demembranated spermatozoa (Fig. 3-4). In terms of Ca^{2+}, flagellar bending was also inhibited but microtubule extrusion was not at high concentrations (10^{-4} M and 10^{-3} M), although microtubule extrusion was inhibited at an extremely high concentration (10^{-2} M of Ca^{2+}) (Fig. 3-7). A previous report showed that flagellar bending was arrested with a sharp bend at 10^{-4} M Ca^{2+} in sea urchin demembranated spermatozoa (Gibbons and Gibbons, 1980), suggesting that microtubules slid to some extent and then arrested at the position at which a sharp bend was formed. Therefore, cAMP and Ca^{2+} might regulate the functions of the components of flagellum such as central apparatus, radial spokes, and dynein, which are involved in the interaction among them and regulate the switching of the active bundles of dynein arms. Supporting this idea, that the partition of the bundles of doublet microtubules was changed by Ca^{2+} concentration (Wargo and Smith, 2003; Nakano *et al*., 2003). Radial spokes contain a nucleoside diphosphate kinase which is stimulated by Ca^{2+} in *Chlamydomonas* flagellum (Patel-King *et al*., 2004). Radial spokes also regulate inner arm dynein through protein phosphorylation and dephosphorylation (Porter and Sale, 2000). Thus, Ca^{2+} exerts its effect *via* protein phosphorylation. On the other hand, PKC was involved in the basal microtubule sliding. By the treatment with PKC inhibitor, microtubule extrusion was completely inhibited (Fig. 3-8). This result suggests that PKC might regulate the structure such as dynein, which is involved in the microtubule sliding. There are some reports showing that dynein heavy chain and light chain are phosphorylated (Bracho *et al*., 1998; Inaba *et al*.,

1999). PKC would be participated in the phosphorylation of dynein arms.

Although cAMP was required for flagellar bending (Fig. 3-4) and its function is mediated *via* protein phosphorylation by PKA (Brandt and Hoskins, 1980; Noland *et al*., 1987; Bookbinder *et al*., 1991), PKA activity was not required for flagellar bending (Fig. 3-4). Therefore, I examined the other targets of cAMP. Epac, an exchange protein directly activated by cAMP, was one of the possible candidates (Kawasaki *et al*., 1998; de Rooij *et al*., 1998). Epac activates Rap family proteins, small GTPases, by transforming them from GDP binding form to GTP binding one (Kitayama *et al*., 1989; Altschuler *et al*., 1995). In this study, I demonstrated that Epac2 and Rap2 are present in hamster spermatozoa (Fig. 3-6). Thus, cAMP would function in the regulation of flagellar bending *via* Epac2/Rap2 pathway. However, the possibility cannot be still excluded that cAMP is mediated by PKA for the regulation of flagellar bending. First, even if the catalytic subunit of PKA is inhibited, the regulatory unit of PKA might play some roles in the regulation of flagellar bending. Second, PKA might exert its effect redundantly with the other mediator of cAMP such as Epac.

Although Ca^{2+} did not affect the flagellar bending of demembranated spermatozoa at a physiological concentration (10^{-7}-10^{-6} M), it has inhibitory effect on microtubule extrusion and flagellar bending in a high concentration (10^{-2} M) (Fig. 3-7). In mouse spermatozoa, the amount of ^{32}P incorporation on overall protein prominently decreased at more than 10^{-3} M of Ca^{2+} concentration (Aoki, 1995). In dog spermatozoa, Ca^{2+} has a detrimental effect on the motility and reduces the overall level of protein phosphorylation (Tash and Means, 1982). These results suggest that protein phosporylation is essential in the flagellar bending and that the decrease in protein phosphorylation level has a detrimental effect on the motility of spermatozoa.

PKC was essential for the microtubule sliding in the demembranated hamster spermatozoa (Fig. 3-8). PKC (protein kinase C) is a family of serine/threonine kinases and has three groups. The first group is conventional PKC isoforms (α, β_I, β_{II}, and γ) that require Ca^{2+} and diacylglycerol (DAG). The second one is novel PKC isoforms (δ, ε,

η, and θ) that are Ca^{2+} independent but require DAG. The third one is atypical PKC isoforms (ζ, ι, λ, and μ) that are independent of either Ca^{2+} or DAG (Hag and Sarre, 1993; Newton, 1997; Neri *et al*., 2002). In the present study, since low Ca^{2+} concentration did not affect the microtubule sliding, the PKC isoform(s) which function in the spermatozoa seems to be the one(s) in novel or atypical PKC group. In the present study, I used the PKC inhibitor which is based on the pseudosubstrate region of PKC (Eichholtz *et al*., 1993). The pseudosubstrate site locates in the regulatory domain interacting with the catalytic domain. The interaction between pseudosubstrate site and the catalytic domain might be important in the regulation of the microtubule sliding.

In the present study, I examined the roles of cAMP, Ca^{2+}, and their targets, *i.e.* PKA and PKC, in the microtubule extrusion and flagellar bending of hamster spermatozoa. The results suggested that cAMP and Ca^{2+} are an essential factor involved in the conversion of microtubule sliding into flagellar bending but not microtubule sliding itself and that PKC is essential for the microtubule sliding independently of Ca^{2+}. In addition, PKA activity is not required for mediating cAMP signal (Fig. 3-9).

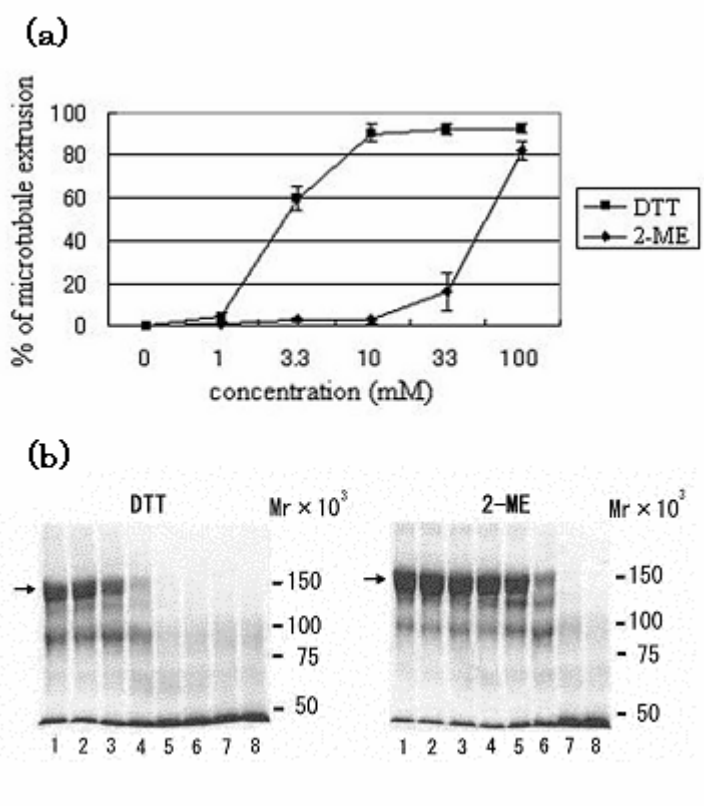

Fig. 3-1. Effects of reducing agents on microtubule extrusion and reduction of the disulfide bonds in IgG. (a) Hamster spermatozoa were treated with different concentrations of dithiothreitol (DTT) or 2-mercaptoethanol (2-ME) in the reactivation medium, and percentages of spermatozoa that had extruded microtubules were determined. Each experiment was conducted three times, and 100 spermatozoa were examined for each replicate at each concentration. The values are expressed as the mean ± S.E.M. (b) SDS- PAGE analysis of IgG for determination of the reducing power of DTT or 2-ME. IgG was incubated for 10 min at 37 ºC in reactivation medium that contained no additives (control; lane 1), or that contained 0.1 mM (lane 2), 0.3 mM (lane 3), 1 mM (lane 4), 3.3 mM (lane 5), 10 mM (lane 6), 33 mM (lane 7), and 100 mM (lane 8) DTT or 2-ME. After incubation, the samples were denatured in Laemmli's SDS sample buffer without 2-ME and separated on SDS-PAGE. Arrows indicate the dense band of intact IgG. The relative molecular masses are shown on the right.

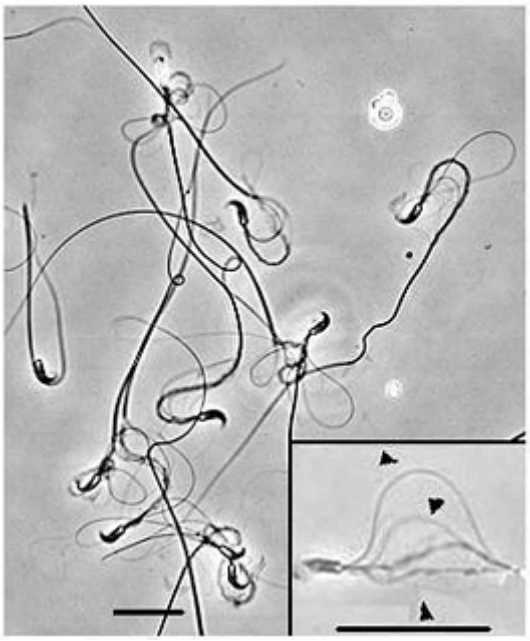

Fig. 3-2. Phase-contrast micrographs of microtubule extrusion. In most of the hamster spermatozoa, microtubules are extruded from the flagellar axonemes. The spermatozoa were photographed after incubation for 10 min in reactivation medium that contained 33 mM DTT. Microtubule extrusion appears on the same side as and/or the opposite side of the curve of the spermatozoal heads in the midpiece region; extruded microtubules are indicated by arrowheads in the lower right corner. Details of the methods used for the induction of microtubule extrusion are described in the *Materials and Methods* section. Scale bars: 20 μm.

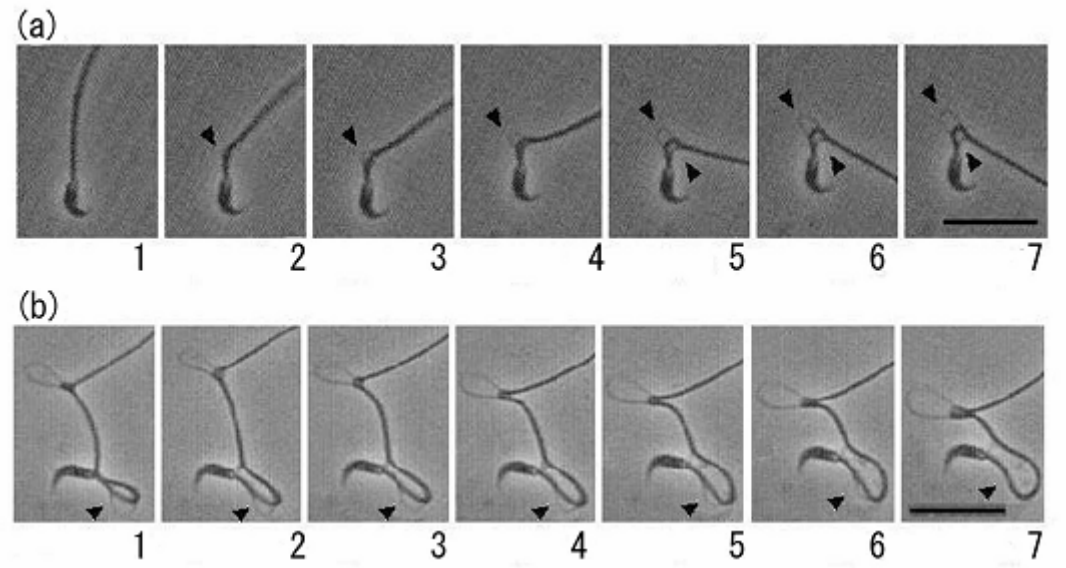

Fig. 3-3. Phase-contrast microscopy images of microtubule extrusion from the flagellar axonemes in hamster spermatozoa. (a) Seven consecutive images were collected at six frames per second. The microtubules that are undergoing extrusion are indicated by arrowheads. (b) Seven consecutive images were collected at the rate of six frames every five seconds. A microtubule that is undergoing intrusion is indicated by the arrowhead. Scale bar: 20 μm.

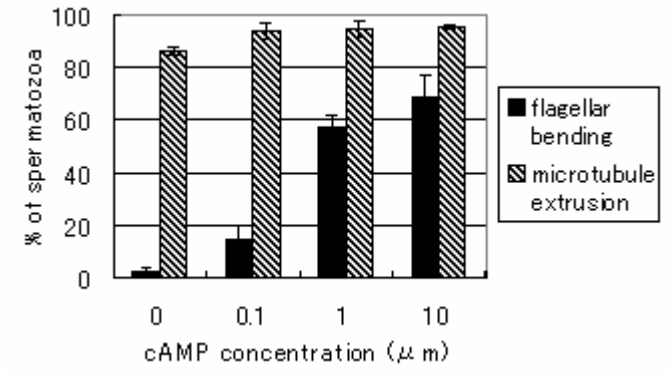

Fig. 3-4. Involvement of cAMP on flaglelar bending and microtubule extrusion in the demembranated spermatozoa. The demembranated spermatozoa were reactivated in the reactivation medium with various concentrations of cAMP. At 0 μM cAMP, 2.0 U/ml cAMP phosphodiesterase was added in the reactivation medium. In the analysis for microtubule extrusion, 33 mM DTT was added in the reactivation medium but not in the analysis for flagellar bending. Percentages of reactivated spermatozoa which showed flagellar bending (solid column) and microtubule extrusion (hatched column) were examined. The experiment was conducted three times. In each experiment, 100 spermatozoa were examined for each cAMP concentration. The values are expressed as the mean ± S.E.M.

Fig. 3-5. Involvement of protein kinase A (PKA) on flaglelar bending and microtubule extrusion in the demembranated spermatozoa. (a) Effects of various concentrations of cAMP on PKA activity. Spermatozoa which had been demembranated and reactivated with various concentrations of cAMP were examined for PKA activity. The experiment was conducted two times and similar results were obtained. Each value is the mean of two experiments. (b) Effects of PKA inhibitor on the flagellar bending. The demembranated spermatozoa were reactivated in the reactivation medium containing 50 μM cAMP with or without 10 μM PKA inhibitor (H-89). Percentages of reactivated spermatozoa which showed flagellar bending were examined. The experiment was conducted three times. In each experiment, 100 spermatozoa were examined for each cAMP concentration. The values are expressed as the mean ± S.E.M. (c) Effects of PKA inhibitor (H-89) on PKA. Spermatozoa which had been demembranated and reactivated in the medium containing 50 μM cAMP with or without PKA inhibitor (H-89) were examined for PKA activity. The experiment was conducted two times and similar results were obtained. Each value is the mean of two experiments.

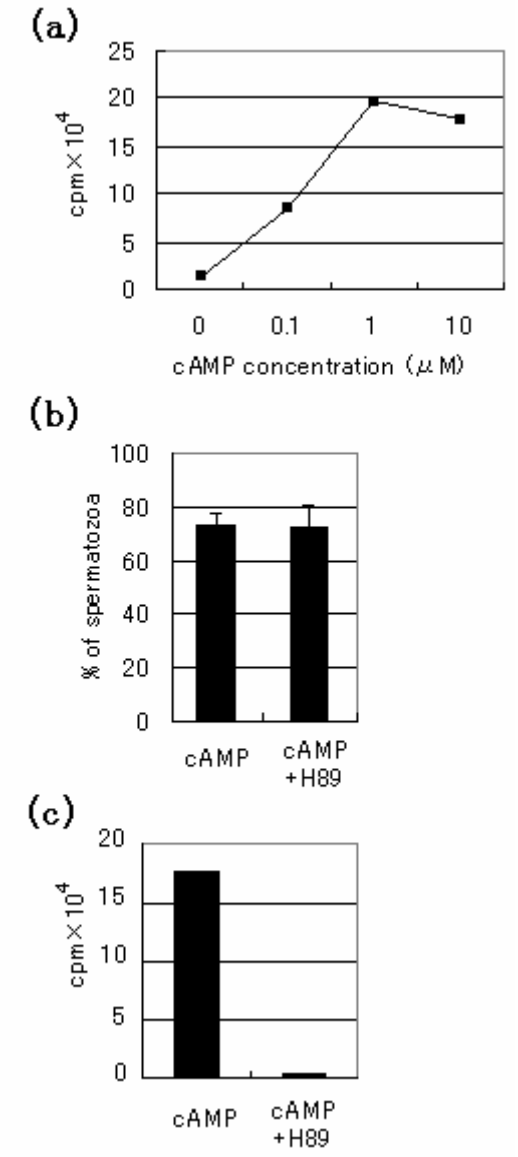
(a)
25
20
15
10
5
0
cpm×10^4
0
0.1
1
10
cAMP concentration (μM)
(b)
100
80
60
40
20
0
% of spermatozoa
cAMP
cAMP +H89
(c)
20
15
10
5
0
cpm×10^4
cAMP
cAMP +H89

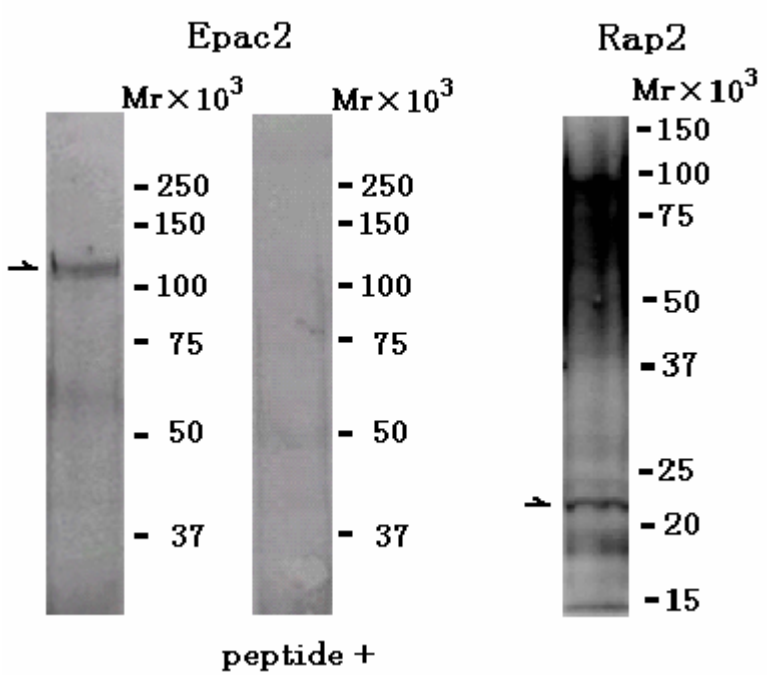

Fig. 3-6. Immunoblotting analysis for Epac/Rap in hamster spermatozoa. Spermatozoa were lysed in extraction buffer and the spermatozoa proteins were separated on SDS-PAGE and probed with anti-Epac2 antibody (Epac2) and anti-Rap2 antibody (Rap2). A specific dense band at 110 kDa for Epac2 and 22 kDa for Rap2, which correspond to their predicted molecular weight, respectively, are indicated by arrows. Anti-Epac2 antibody was neutralized with antigen peptide, which is shown in the right column (peptide+). Molecular mass standards are indicated to the right of the lanes. The experiment was conducted three times and similar results were obtained.

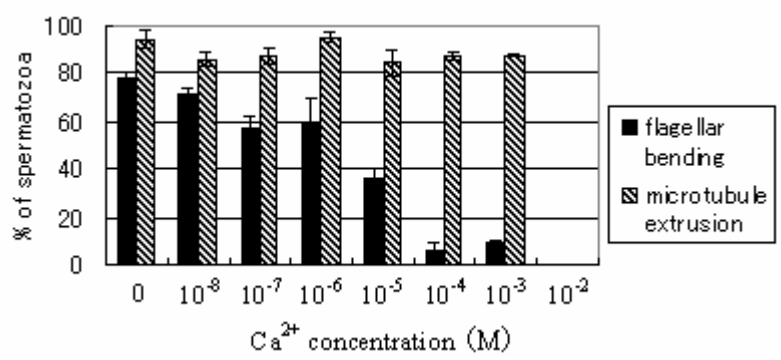

Fig. 3-7. Effects of Ca^{2+} on flagellar bending and microtubule extrusion in the demembranated hamster spermatozoa. The demembranated spermatozoa were reactivated in the reactivation medium containing various concentrations of Ca^{2+} with or without 33 mM DTT in the analysis for microtubule extrusion or flagellar bending, respectively. Percentage of reactivated spermatozoa which showed flagellar bending (solid column) and microtubule extrusion (hatched column) are shown in the figure. The experiment was conducted two times. In each experiment, 100 spermatozoa were examined at each calcium concentration. The values are expressed as the mean ± S.E.M.

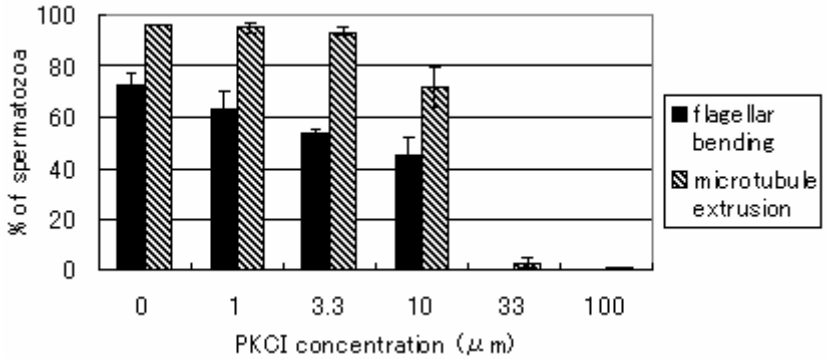

Fig. 3-8. Involvement of Protein kinase C (PKC) on flagellar bending and microtubule extrusion in the demembranated hamster spermatozoa. The demembranated spermatozoa were reactivated in the reactivation medium containing PKC inhibitor (PKCI) with or without 33 mM DTT in the analysis for microtubule extrusion or flagellar bending, respectively. Percentage of reactivated spermatozoa which showed flagellar bending (solid column) and microtubule extrusion (hatched column) are shown in the figure. The experiment was conducted three times. In each experiment, 100 spermatozoa were examined at each PKCI concentration. The values are expressed as the mean ± S.E.M.

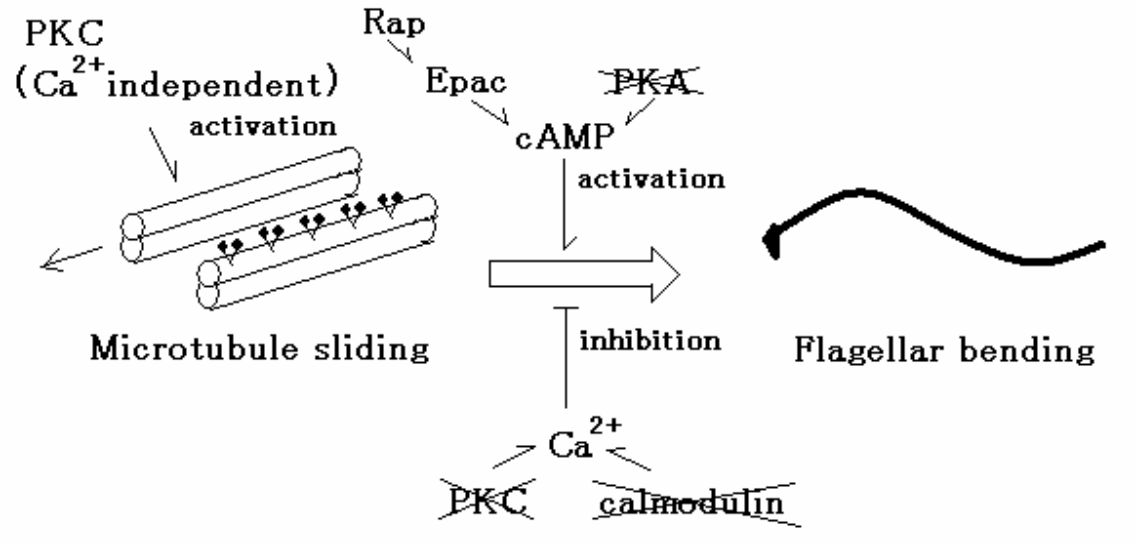

Fig. 3-9. Hypothesis of the mechanism by which microtubule sliding is converted into flagellar bending. PKC is essential for the microtubule sliding independently of Ca^{2+}. Cyclic AMP is essential for the conversion of microtubule sliding into flagellar bending. The target of cAMP is not PKA. Alternatively, Epac2/Rap2 pathway would mediate the signal of cAMP to regulate flagellar bending. Ca^{2+} has inhibitory effect for the conversion of microtubule sliding into flagellar bending. The target of Ca^{2+} is neither PKC nor calmodulin.

General Discussion and Future Perspective

Spermatozoa are the one of two principal parts in fertilization and their role is to bring a haploid genome into the egg. For the accomplishment of fertilization, spermatozoa are necessary to swim actively to reach an oocyte. Therefore, it is important to elucidate the mechanism regulating the motility in spermatozoa. The motility for the progressive movement is generated by flagellar bending, which is regulated *via* the conversion of microtubule sliding into flagellar bending. In the present study, I investigated the mechanisms by which microtubule sliding is converted into flagellar bending and then flagellar bending generates the motility of spermatozoa. Hyperactivation is a good model for investigation of the mechanism by which flagellar bending generate the motility of spermatozoa since the propulsive force for the movement is enhanced. To investigate this mechanism, I quantitatively analyzed the motility and flagellar bending in hyperactivated hamster spermatozoa. In these analyses, I clarified the characteristics of movement and flagellar bending in hyperactivated spermatozoa and elucidated how they produce the large propulsive force. To investigate the mechanism for the conversion of microtubule sliding into flagellar bending, I developed the analytical method to separately examine the microtubule sliding and flagellar bending in demembranated hamster spermatozoa. Using this method, I clarified that cAMP and Ca^{2+} were involved in the conversion and PKC was involved in the microtubule sliding.

Hyperactivation is a good model for investigation of the mechanism by which flagellar bending generate the motility of spermatozoa. In the present study, I identified the characteristics of hyperactivation which are formed by two factors as shown in chapter 1 and 2. First, hyperactivated spermatozoa lose the straightness of the path (Figs. 1-2, 1-3d, and 1-3e in chapter 1), which is caused by the increase in asymmetrical flagellar bending to the direction of R-bend (Figs. 2-3 and 2-4b in chapter 2). Second, the swimming speed increases (Figs. 1-3b, 1-3c in chapter 1) and the progressive

motility is enhanced in the viscoelastic medium (Fig. 1-5 in chapter 1). These seem to be caused by the increase in the propulsive force with the large effective strokes derived from the high amplitude after the onset of hyperactivation (Fig.2-13 in chapter 2). Furthermore, the disappearance of interference waves seems to contribute the increase in the propulsive force (Figs. 2-7 and 2-8 in chapter 2).

In the analysis for the propagation of waves, I found that the wave arose cyclically and is propagated from the basal region to the tip (Fig. 2-6 in chapter 2). This suggests that there is the pacemaker regulating the cyclical oscillation of beating. Although the additional waves arose in the mid region in the spermatozoa incubated for 10 min, they were also propagated to the tip as well as the large wave that arose in the basal region. This result suggests that the pacemakers localize in not only the basal region but also other regions on the flagellum. This is plausible because dynein arms themselves are oscillating force generator (Shingyoji et al., 1998), suggesting that the pacemaker localized in all regions of the flagellum. In hyperactivated spermatozoa in which the propulsive force for the movement is enhanced, the wave arose only in the base of the flagellum and no additional waves was observed. This would be helpful to produce the large propulsive force, since additional waves interfere in the formation of complete cycle of the large wave. It is possible that there is a mechanism regulating the position of pacemaker, and that changes in this mechanism are involved in the occurrence of hyperactivation.

The mechanism by which the interactions among the components of axoneme structure generate the propulsive force remains unclear. In the present study, I showed that the high amplitude is essential for generating the large propulsive force. To produce the high amplitude, microtubules should continue to slide to one direction for a long time to slide a long distance and the decrease in the beat frequency would be the major contributor for it. Therefore, the longer pace of alternating switching from the sliding of one side to that of the opposite side produces the higher amplitude. The mechanism regulating the alternating switching was explained by “Geometric Clutch Hypothesis”

proposed by Lindemann (1994), as that the dynein arms alternatingly attach and detach to the microtubules between one side of the active bundle of microtubules and the opposite side of the inactive one, respectively. Based on this hypothesis, I propose the following hypothesis for the mechanism regulating the pace of alternating switching. The distance between the dynein and the adjacent microtubule would regulate the pace of switching. The central apparatuses such as radial spokes would contribute the size in the circumference of the circle built by 9 outer doublet microtubules. The structure of these apparatuses would be changed by the post-translational regulation such as the protein phosphorylation. As the results in the structural change of the central apparatuses, each distance between the dynein and the adjacent doublet microtubule would be changed. Supporting this hypothesis, a previous report suggested that the gene product of *pf-27* is involved in the phosphorylation of radial spoke polypeptides in *Chlamydomonas* (Huang *et al*., 1981). In chapter 3, I showed that cAMP and Ca^{2+} are involved in the conversion of microtubule sliding into flagellar bending. These factors may be involved in the structural change of central apparatuses such as radial spokes. It has been reported that flagellar radial spoke protein 2 and 3 function as a calmodulin binding protein and a cAMP dependent kinase anchoring protein, respectively, and that these proteins are required for the motility (Yang *et al*., 2004; Gaillard *et al*., 2001).

The mechanism by which dynein arms generate the sliding of microtubules seems to involve their structural changes. A recent study for *Chlamydomonas* flagella showed the details in the structural changes of dynein between the start and end of power stroke (Burgess et al., 2003). In the system of myosin/actin, the motor domain but not the neck domain of ATPase myosin-V, which is an equivalent of dynein in the system of dynein/microtubule, determines the sliding movement of the actin filament (Tanaka et al., 2002). Thus, the structural changes in dynein arms would alter their activity and regulate the sliding of microtubules. In the present study, I showed that microtubule sliding is regulated by PKC, independently of Ca^{2+} (Fig. 3-7 and 3-8 in chapter 3). Several reports showed that dynein heavy chain and light chain are

phosphorylated with the activation of the motility (Dey and Brokaw, 1991; Bracho *et al*., 1998; Inaba *et al*., 1999). Therefore, PKC might phosphorylate dynein independently of Ca^{2+}, to induce the structural changes in dynein arms.

The Reynolds number is important in analyzing various types of flow. The power output derived from the wave is dependent on the Reynolds number. The Reynolds number of the system in the environment around human-beings is over 10^3, while the one around spermatozoa is approximately 10^{-3} (Jahn and Votta, 1972). Currently, little is known about the power output derived from the waves in such a low Reynolds number environment. In the present study, I showed that the hamster spermatozoa efficiently progresses by producing the effective and ineffective strokes. Thus, the spermatozoa are a good model for elucidating the mechanism by which the waveform generates the power output in a low Reynolds number environment. This knowledge would be useful for the development of the automated micro-machine in the future.

Acknowledgements

I would like to express my acknowledgement to Dr. Fugaku Aoki for his all support, providing an opportunity to study this work, encouragement, helpful advice and etc. I appreciate Dr. Makoto Okuno at the University of Tokyo for helpful discussion and encouragement. I also appreciate Dr. Shoji Baba and Dr. Junko Ohmuro at Ochanomizu University for providing Bohboh exe, helpful discussion and encouragement. I also express my acknowledgement to Dr. Masao Nagata and to other members of Laboratory of Bioresource Regulation and members of Laboratory of Animal Breeding for their all support. Finally I would like to express my acknowledgement to my parents, Akira and Chiyoko, and to my wife, Megumi, for having been supporting me in various aspects.

References

Altschuler DL, Peterson SN, Ostrowski MC, Lapetina EG (1995) Cyclic AMP-dependent activation of Rap1b *Journal of Biological Chemistry* **270** 10373-10376.

Aoki F (1995) Mechansim of hyperactivation in hamster and mouse sperm *Doctor thesis on the Graduate school of Agricultural and Life sciences, The University of Tokyo*

Aoki F, Ishida K, Okuno M, Kohmoto K (1994) Analysis of flagellar bending in hyperactivated hamster and mouse spermatozoa *Journal of Reproduction and Fertility* **101** 397-403

Ashizawa K, Katayama S, Tsuzuki Y (1992) Regulation of flagellar motility by temperature-dependent phosphorylation of a 43 kDa axonemal protein in fowl spermatozoa *Biochemical and Biophysical Research Communications* **185** 740-745

Ashizawa K, Tomonaga H, Tsuzuki Y (1994) Regulation of flagellar motility of fowl spermatozoa: evidence for the involvement of intracellular free Ca^{2+} and calmodulin *Journal of Reproduction and Fertility* **101** 265-272

Bannai H, Yoshimura M, Takahashi K, Shingyoji C (2000) Calcium regulation of microtubule sliding in reactivated sea urchin sperm flagella *Journal of Cell Science* **113** 831-839

Bessen M, Fay RB, Witman GB (1980) Calcium control of waveform in isolated flagellar axonemes of Chlamydomonas *The Journal of Cell Biology* **86** 446-455

Bookbinder LH, Moy GW, Vacquier VD (1991) In vitro phosphorylation of sea urchin sperm adenylate cyclase by cyclic adenosine monophosphate-dependent protein

kinase *Molecular Reproduction and Development* **28** 150-157

Brandt H, Hoskins DD (1980) A cAMP-dependent phosphorylated motility protein in bovine epididymal sperm *Journal of Biological Chemistry* **255** 982-987

Brokaw CJ Calcium-induced asymmetrical beating of triton-demembranated sea urchin sperm flagella (1979) *The Journal of Cell Biology* **82** 401-411.

Brokaw CJ (1980) Elastase digestion of demembranated sperm flagella *Science* **207** 1365-1367

Brokaw CJ (2002) Computer simulation of flagellar movement VIII: coordination of dynein by local curvature control can generate helical bending waves *Cell Motility and Cytoskeleton* **53** 103-124

Brokaw CJ, Josslin R, Bobrow L (1974) Calcium ion regulation of flagellar beat symmetry in reactivated sea urchin spermatozoa *Biochemical and Biophysical Research Communications* **58** 795-800.

Brokaw CJ, Simonick TF (1977) Motility of triton-demembranated sea urchin sperm flagella during digestion by trypsin *The Journal of Cell Biology* **75** 650-665

Bracho GE, Fritch JJ, Tash JS (1998) Identification of flagellar proteins that initiate the activation of sperm motility in vivo *Biomedical and Biophysical Research Communication* **242** 231-237

Burgess SA, Walker ML, Sakakibara H, Knight PJ, Oiwa K (2003) Dynein structure and power stroke *Nature* **421** 715-718

Burks DJ, Carballada R, Moore HD, Saling PM (1995) Interaction of a tyrosine kinase from human sperm with the zona pellucida at fertilization *Science* **269** 83-86

Cancel AM, Lobdell D, Mendola P, Perreault SD (2000) Objective evaluation of hyperactivated motility in rat spermatozoa using computer-assisted sperm

analysis *Human Reproduction* **15** 1322-1328

Carrera A, Gerton GL, Moss SB (1994) The major fibrous sheath polypeptide of mouse sperm: structural and functional similarities to the A-kinase anchoring proteins *Developmental Biology* **165** 272-284

Cheng YS, Chen LB (1981) Detection of phosphotyrosine-containing 34,000-dalton protein in the framework of cells transformed with Rous sarcoma virus *Proceedings of the National Academy of Sciences of the United States of America* **78** 2388-2392

Cooper JA, Hunter T (1981) Four different classes of retroviruses induce phosphorylation of tyrosines present in similar cellular proteins *Molecular and Cellular Biology* **1** 394-407

de Rooij J, Zwartkruis FJ, Verheijen MH, Cool RH, Nijman SM, Wittinghofer A, Bos JL (1998) Epac is a Rap1 guanine-nucleotide-exchange factor directly activated by cyclic AMP *Nature* **396** 474-477

Dey CS, Brokaw CJ (1991) Activation of Ciona sperm motility: phosphorylation of dynein polypeptides and effects of a tyrosine kinase inhibitor *Journal of Cell Science* **100** 815-824

Drobnis EZ, Yudin AI, Cherr GN, Katz DF (1988) Kinematics of hamster sperm during penetration of the cumulus cell matrix *Gamete Research* **21** 367-383

Eichholtz T, de Bont DB, de Widt J, Liskamp RM, Ploegh HL A myristoylated pseudosubstrate peptide, a novel protein kinase C inhibitor *Journal of Biological Chemistry* **268** 1982-1986.

Enserink JM, Price LS, Methi T, Mahic M, Sonnenberg A, Bos JL, Tasken K (2004) The cAMP-Epac-Rap1 pathway regulates cell spreading and cell adhesion to laminin-5 through the alpha3beta1 integrin but not the alpha6beta4 integrin *Journal of Biological Chemistry* **279** 44889-44896

Fraser LR (1977) Motility patterns in mouse spermatozoa before and after capacitation *Journal of Experimental Zoology* **202** 439-444

Gaillard AR, Diener DR, Rosenbaum JL, Sale WS (2001) Flagellar radial spoke protein 3 is an A-kinase anchoring protein (AKAP) *The Journal of Cell Biology* **153** 443-448

Gibbons BH (1982) Effects of organic solvents on flagellar asymmetry and quiescence in sea urchin sperm *Journal of Cell Science* **54** 115-35

Gibbons BH, Gibbons IR (1980) Calcium-induced quiescence in reactivated sea urchin sperm *The Journal of Cell Biology* **84** 13-27

Goldstein DA (1979) Calculation of the concentration of free cations and cation-ligand complexes in solutions containing multiple divalent cations and ligands *Biophysical Journal* **26** 235-242

Gray J, Hancock G.J (1955) The propulsion of sea-urchin spermatozoa *Journal of Experimental Biology* **32** 802-814.

Gray J (1958) The movement of the spermatozoa of the bull *Journal of Experimental Biology* **35** 96-108

Hancock GJ (1953) The self-propulsion of microscopic organisms *Proceedings of The Royal Society A* **217** 96-121

Hayashi H, Yamamoto K, Yonekawa H, Morisawa M (1987) Involvement of tyrosine protein kinase in the initiation of flagellar movement in rainbow trout spermatozoa *Journal of Biological Chemistry* **262** 16692-16698

Haystead TA, Weiel JE, Litchfield DW, Tsukitani Y, Fischer EH, Krebs EG (1990) Okadaic acid mimics the action of insulin in stimulating protein kinase activity in isolated adipocytes. The role of protein phosphatase 2a in attenuation of the signal. *Journal of Biological Chemistry* **265** 16571-16580

Ho HC, Suarez SS (2001) Hyperactivation of mammalian spermatozoa: function and regulation *Reproduction* **122** 519-526

Holwill ME, Satir P (1994) Physical model of axonemal splitting *Cell Motility and the Cytoskeleton* **27** 287-298

Huang B, Piperno G, Ramanis Z, Luck DJ (1981) Radial spokes of Chlamydomonas flagella: genetic analysis of assembly and function *The Journal of Cell Biology* **88** 80-88

Hug H, Sarre TF (1993) Protein kinase C isoenzymes: divergence in signal transduction? *Biochemical Journal* **291** 329-343

Inaba K (2003) Molecular architecture of the sperm flagella: molecules for motility and signaling *Zoological Science* **20** 1043-1056

Inaba K, Kagami O, Ogawa K (1999) Tctex2-related outer arm dynein light chain is phosphorylated at activation of sperm motility *Biochemical and Biophysical Research Communications* **256** 177-183

Ishida K, Okuno M, Morisawa S, MohriT, Mohri H, Waku M, Morisawa M (1987) Initiation of sperm motility induced by cyclic AMP in hamster and boar *Development, Growth and Differentiation* **29** 47-56

Ishiguro K, Murofushi H, Sakai H (1982) Evidence that cAMP-dependent protein kinase and a protein factor are involved in reactivation of triton X-100 models of sea urchin and starfish spermatozoa *The Journal of Cell Biology* **92** 777-782

Ishijima S, Baba S, Mohri H, Suarez SS (2002) Quantitative analysis of flagellar movement in hyperactivated and acrosome-reacted golden hamster spermatozoa *Molecular Reproduction and Development* **61** 376-384

Ishijima S, Iwamoto T, Nozawa S, Matsushita K (2002) Motor apparatus in human spermatozoa that lack central pair microtubules *Molecular Reproduction and*

Development **63** 459-463

Ishijima S. Mohri (1985) A quantitative description of flagellar movement in golden hamster spermatozoa *Journal of Experimental Biology* **114** 463-475

Ishijima S, Witman GB (1991) Demembranation and reactivation of mammalian spermatozoa from golden hamster and ram *Methods in Enzymology* **196** 417-428

Jahn TL, Votta JJ (1972) Locomotion of protozoa *Annual Review of Fluid Mechanics* **4** 93-116

Johnson LL, Katz DF, Overstreet JW (1981) The movement characteristics of rabbit spermatozoa before and after activation *Gamete Research* **4** 275-282

Kamiya R, Witman GB (1984) Submicromolar levels of calcium control the balance of beating between the two flagella in demembranated models of Chlamydomonas *The Journal of Cell Biology* **98** 97-107

Katz DF, Cherr GN, Lambert H (1986) The evalution of hamster sperm motility during capacitation and interaction with ovum vestments in vitro *Gamete Research* **14** 333-346

Katz DF, Yanagimachi R (1980) Movement characteristics of hamster spermatozoa within the oviduct *Biology of Reproduction* **22** 759-764.

Katz DF, Yanagimachi R, Dresdner RD (1978) Movement characteristics and power output of guinea-pig and hamster spermatozoa in relation to activation *Journal of Reproduction and Fertility* **52** 167-172

Kawasaki H, Springett GM, Mochizuki N, Toki S, Nakaya M, Matsuda M, Housman DE, Graybiel AM (1998) A family of cAMP-binding proteins that directly activate Rap1 *Science* **282** 2275-2279.

Kemp BE, Graves DJ, Benjamini E, Krebs EG (1977) Role of multiple basic residues in determining the substrate specificity of cyclic AMP-dependent

protein kinase *Journal of Biological Chemistry* **252** 4888-4894

Kinukawa M, Nagata M, Aoki F (2004) Reducing agents induce microtubule extrusion in demembranated mammalian spermatozoa *Reproduction* **128** 813-818

Kitayama H, Sugimoto Y, Matsuzaki T, Ikawa Y, Noda M (1989) A ras-related gene with transformation suppressor activity *Cell* **56** 77-84.

Kula Nand J, Shivaji S (2002) Identification of the major tyrosine phosphorylated protein of capacitated hamster spermatozoa as a homologue of mammalian sperm A kinase anchoring protein *Molecular Reproduction and Development* **61** 258-270

Laemmli UK (1970) Cleavage of structural proteins during the assembly of the head of bacteriophage T4 *Nature* **227** 680-685

Lindemann CB (1978) A cAMP-induced increase in the motility of demembranated bull sperm models *Cell* **13** 9-18

Lindemann CB, Gardner TK, Westbrook E, Kanous KS (1991) The calcium-induced curvature reversal of rat sperm is potentiated by cAMP and inhibited by anti-calmodulin *Cell Motility and the Cytoskeleton* **20** 316-324

Lindemann CB, Gibbons IR (1975) Adenosine triphosphate-induced motility and sliding of filaments in mammalian sperm extracted with Triton X-100 *The Journal of Cell Biology* **65** 147-162

Lindemann CB, Orlando A, Kanous KS (1992) The flagellar beat of rat sperm is organized by the interaction of two functionally distinct populations of dynein bridges with a stable central axonemal partition *Journal of Cell Science* **102** 249-260

Lindemann CB (1994) A model of flagellar and ciliary functioning which uses the

forces transverse to the axoneme as the regulator of dynein activation *Cell Motility and the Cytoskeleton* **29** 141-154

Luconi M, Baldi E (2003) How do sperm swim? Molecular mechanisms underlying sperm motility *Cellular and Molecular Biology (Noisy-le-grand)* **49** 357-369

Mcgrath J, Hillman N, Nadijcka M (1977) Separation of dead and live mouse spermatozoa *Developmental Biology* **61** 114-117

Miki K, Willis WD, Brown PR, Goulding EH, Fulcher KD, Eddy EM (2002) Targeted disruption of the Akap4 gene causes defects in sperm flagellum and motility *Developmental Biology* **248** 331-342

Morales P, Overstreet JW, Katz DF (1988) Changes in human sperm motion during capacitation in vitro *Journal of Reproduction and Fertility* **83** 119-128

Morisawa M, Hayashi H (1986) Phosphorylation of a 15K axonemal protein in the trigger initiating trout sperm motility *Biomedical Research* **6** 181-184

Morisawa M, Okuno M (1982) Cyclic AMP induces maturation of trout sperm axoneme to initiate motility *Nature* **295** 703-704

Mortimer ST, Swan MA (1995) Kinematics of capacitating human spermatozoa analyzed at 60 Hz *Human Reproduction* **10** 873-879

Mortimer ST, Maxwell WM (1999) Kinematic definition of ram sperm hyperactivation *Reproduction, Fertility and Development* **11** 25-30

Moss SB, Turner RM, Burkert KL, VanScoy Butt H, Gerton GL (1999) Conservation and function of a bovine sperm A-kinase anchor protein homologous to mouse AKAP82 *Biology of Reproduction* **61** 335-342

Nakano I, Kobayashi T, Yoshimura M, Shingyoji C (2003) Central-pair-linked regulation of microtubule sliding by calcium in flagellar axonemes *Journal of Cell Science* **116** 1627-1636

Neill JM, Olds-Clarke P (1987) A computer-assisted assay for mouse sperm hyperactivation demonstrates that bicarbonate but not bovine serum albumin is required *Gamete Research* **18** 121-140

Neri LM, Borgatti P, Capitani S, Martelli AM (2002) Protein kinase C isoforms and lipid second messengers: a critical nuclear partnership? *Histology and Histopathology* **17** 1311-1316

Neugebauer DC, Neuwinger J, Jockenhovel F, Nieschlag E (1990) '9+0' axoneme in spermatozoa and some nasal cila of a patient with totally immotile spermatozoa associated with thickened sheath and short midpiece *Human Reproduction* **5** 981-986

Newton AC (1997) Regulation of protein kinase C *Current Opinion in Cell Biology* **9** 161-167

Niitsu-Hosoya N, Ishida K, Mohri H (1987) Change in intracellular concentration of cyclic nucleotides during the initiation process of starfish motility *Development, Growth and Differentiation* **29** 563-569

Noland TD, Abumrad NA, Beth AH, Garbers DL (1987) Protein phosphorylation in intact bovine epididymal spermatozoa: identification of the type II regulatory subunit of cyclic adenosine 3',5'-monophosphate-dependent protein kinase as an endogenous phosphoprotein *Biology of Reproduction* **37** 171-180

Nomura M, Yoshida M, Morisawa M (2004) Calmodulin/calmodulin-dependent protein kinase II mediates SAAF-induced motility activation of ascidian sperm *Cell Motility and Cytoskeleton* **59** 28-37

Olson GE, Linck RW (1977) Observation of the structural components of flagellar axonemes and central pair microtubules from rat sperm *Journal of Ultrastructure Research* **61** 21-43

Opresko LK, Brokaw CJ (1983) cAMP-dependent phosphorylation associated with

activation of motility of ciona sperm flagella *Gamete Research* **8** 201-218

Porter ME, Sale WS (2000) The 9+2 axoneme anchors multiple inner arm dyneins and a network of kinases and phosphatases that control motility *The Journal of Cell Biology* **151** F37-F42

Rangarajan S, Enserink JM, Kuiperij HB, de Rooij J, Price LS, Schwede F, Bos JL (2003) Cyclic AMP induces integrin-mediated cell adhesion through Epac and Rap1 upon stimulation of the beta 2-adrenergic receptor *The Journal of Cell Biology* **160** 487-493

Ren D, Navarro B, Perez G, Jackson AC, Hsu S, Shi Q, Tilly JL, Clapham DE (2001) A sperm ion channel required for sperm motility and male fertility *Nature* **413** 603-609

Satir P (1985) Switching mechanisms in the control of ciliary motility *In Modern Cell Biology* (ed. B. Satir) A. R. Liss, NY 1-46

Sale WS, Satir P (1977) Direction of active sliding of microtubules in Tetrahymena cilia *Proceedings of the National Academy of Sciences* **74** 2045-2049

Satir, SaleWS (1977) Tails of Tetrahymena *Journal of Protozoology* **24** 498-501

Shingyoji C, Higuchi H, Yoshimura M, Katayama E, Yanagida T (1998) Dynein arms are oscillating force generators *Nature* **393** 711-4.

Shingyoji C, Murakami A, Takahashi K (1977) Local reactivation of Triton-extracted flagella by iontophoretic application of ATP *Nature* **265** 269-270

Shivaji S, Peedicayil J, Girija Devi L (1995) Analysis of the motility parameters of in vitro hyperactivated hamster spermatozoa *Molecular Reproduction and Development* **42** 233-247

Si Y, Okuno M (1993) The sliding of the fibrous sheath through the axoneme proximally together with microtubule extrusion *Experimental Cell Research* **208**

170-174

Si Y, Okuno M (1995) Extrusion of microtubule doublet outer dense fibers 5-6 associating with fibrous sheath sliding in mouse sperm flagella *Journal of Experimental Zoology* **273** 355-362

Smith EF (2002) Regulation of flagellar dynein by calcium and a role for an axonemal calmodulin and calmodulin-dependent kinase *Molecular and Cellular Biology* **13** 3303-3313

Sturgess JM, Chao J (1982) Ultrastructural features of a human genetic defect of cilia *Progress in Clinical and Biological Research* **80** 7-12

Stauss CR, Votta TJ, Suarez SS Sperm motility hyperactivation facilitates penetration of the hamster zona pellucida (1995) *Biology of Reproduction* **53** 1280-1285

Suarez SS (1988) Hamster sperm motility transformation during development of hyperactivation in vitro and epididymal maturation *Gamete Research* **19** 51-65

Suarez SS, Dai X (1992) Hyperactivation enhances mouse sperm capacity for penetrating viscoelastic media *Biology of Reproduction* **46** 686-691

Suarez SS, Katz DF, Owen DH, Andrew JB, Powell RL (1991) Evidence for the function of hyperactivated motility in sperm *Biology of Reproduction* **44** 375-381

Suarez SS, Katz DF, Overstreet JW (1983) Movement characteristics and acrosomal status of rabbit spermatozoa recovered at the site and time of fertilization. *Biology of Reproduction* **29** 1277-1287.

Suarez SS, Osman RA (1987) Initiation of hyperactivated flagellar bending in mouse sperm within the female reproductive tract *Biology of Reproduction* **36** 1191-1198.

Summers KE, Gibbons IR (1973) Effect of trypsin digestion on flagellar structures

and their relationship to motility *The Journal of Cell Biology* **58** 618-629

Tamm SL. Tamm S (1984) Alternate patterns of doublet microtubule sliding in ATP-disintegrated macrocilia of the ctenophore Beroe *The Journal of Cell Biology* **99** 1364-1371

Tanaka H, Homma K, Iwane AH, Katayama E, Ikebe R, Saito J, Yanagida T, Ikebe M (2002) The motor domain determines the large step of myosin-V *Nature* **415** 192-195.

Tash JS, Hidaka H, Means AR (1986) Axokinin phosphorylation by cAMP-dependent protein kinase is sufficient for activation of sperm flagellar motility *The Journal of Cell Biology* **103** 649-655

Tash JS, Kakar SS, Means AR (1984) Flagellar motility requires the cAMP-dependent phosphorylation of a heat-stable NP-40-soulble 56 kd protein, axokinin *Cell* **38** 551-559

Tash JS, Means AR (1982) Regulation of protein phosphorylation and motility of sperm by cyclic adenosine monophosphate and calcium *Biology of Reproduction* **26** 745-763

Tash JS, Means AR (1987) Ca^{2+} regulation of sperm axonemal motility *Methods in Enzymology* **139** 808-823

Tessler S, Olds-Clarke P (1985) Linear and nonlinear mouse sperm motility patterns. A quantitative classification. *Journal of Andrology* **6** 35-44

Visconti PE, Moore GD, Bailey JL, Leclerc P, Connors SA, Pan D, Olds-Clarke P, Kopf GS (1995) Capacitation of mouse spermatozoa. II. Protein tyrosine phosphorylation and capacitation are regulated by a cAMP-dependent pathway *Development* **121** 1139-1150

Wargo MJ, Smith EF (2003) Asymmetry of the central apparatus defines the location

of active microtubule sliding in Chlamydomonas flagella *Proceedings of the National Academy of Sciences of the United States of America* **100** 137-142.

White DR, Aitken RJ (1989) Relationship between calcium, cyclic AMP, ATP, and intracellular pH and the capacity of hamster spermatozoa to express hyperactivated motility *Gamete Research* **22** 163-177

Wiesner B, Weiner J, Middendorff R, Hagen V, Kaupp UB, Weyand I (1998) Cyclic nucleotide-gated channels on the flagellum control Ca2+ entry into sperm *The Journal of Cell Biology* **142** 473-484

Witman GB, Plummer J, Sander G (1978) Chlamydomonas flagellar mutants lacking radial spokes and central tubules. Structure, composition, and function of specific axonemal component *The Journal of Cell Biology* **76** 729-747

Woolley DM (1977) Evidence for "twisted plane" undulations in golden hamster sperm tails *The Journal of Cell Biology* **75** 851-865

Woolley DM (2000) The molecular motors of cilia and eukaryotic flagella *Essays in Biochemistry* **35** 103-115

Yanagimachi R (1970) The movement of golden hamster spermatozoa before and after capacitation *Journal of Reproduction and Fertility* **23** 193-196

Yanagimachi R (1981) Mechanisms of fertilization in mammals. In *Fertilization and Embryonic Development in vitro* pp81-182 Eds L Mastroianni and JD Biggers.: Plenum Press, New York

Yanagimachi R (1994) Mammlian fertilization. In *The Physiology of Reproduction*: pp189-317 Eds E Knobil and JD Neill.: Raven Press, New York

Yang P, Yang C, Sale WS (2004) Flagellar radial spoke protein 2 is a calmodulin binding protein required for motility in Chalamydomonas reinhardtii *Eukaryotic Cell* **3** 72-81

Yudin AI, Cherr GN, Katz DF (1988) Structure of the cumulus matrix and zona pellucida in the golden hamster: a new view of sperm interaction with oocyte-associated extracellular matrices *Cell Tissue Research* **251** 555-564